Neuromuscular synapse integrity requires linkage of acetylcholine receptors to postsynaptic intermediate filament networks via rapsyn–plectin 1f complexes

Eva Mihailovska[a], Marianne Raith[a], Rocio G. Valencia[a], Irmgard Fischer[a], Mumna Al Banchaabouchi[b], Ruth Herbst[c], and Gerhard Wiche[a]

[a]Department of Biochemistry and Cell Biology, Max F. Perutz Laboratories, University of Vienna, 1030 Vienna, Austria; [b]Preclinical Phenotyping Facility, Campus Science Support Facilities, 1030 Vienna, Austria; [c]Center for Brain Research and Institute of Immunology, Medical University of Vienna, 1030 Vienna, Austria

ABSTRACT **Mutations in the cytolinker protein plectin lead to grossly distorted morphology of neuromuscular junctions (NMJs) in patients suffering from epidermolysis bullosa simplex (EBS)-muscular dystrophy (MS) with myasthenic syndrome (MyS). Here we investigated whether plectin contributes to the structural integrity of NMJs by linking them to the postsynaptic intermediate filament (IF) network. Live imaging of acetylcholine receptors (AChRs) in cultured myotubes differentiated ex vivo from immortalized plectin-deficient myoblasts revealed them to be highly mobile and unable to coalesce into stable clusters, in contrast to wild-type cells. We found plectin isoform 1f (P1f) to bridge AChRs and IFs via direct interaction with the AChR-scaffolding protein rapsyn in an isoform-specific manner; forced expression of P1f in plectin-deficient cells rescued both compromised AChR clustering and IF network anchoring. In conditional plectin knockout mice with gene disruption in muscle precursor/satellite cells (Pax7-Cre/cKO), uncoupling of AChRs from IFs was shown to lead to loss of postsynaptic membrane infoldings and disorganization of the NMJ microenvironment, including its invasion by microtubules. In their phenotypic behavior, mutant mice closely mimicked EBS-MD-MyS patients, including impaired body balance, severe muscle weakness, and reduced life span. Our study demonstrates that linkage to desmin IF networks via plectin is crucial for formation and maintenance of AChR clusters, postsynaptic NMJ organization, and body locomotion.**

Monitoring Editor
Thomas M. Magin
University of Leipzig

Received: Jun 30, 2014
Revised: Oct 8, 2014
Accepted: Oct 9, 2014

This article was published online ahead of print in MBoC in Press (http://www.molbiolcell.org/cgi/doi/10.1091/mbc.E14-06-1174) on October 15, 2014.

Address correspondence to: Gerhard Wiche (gerhard.wiche@univie.ac.at).

Abbreviations used: ABD, actin-binding domain; AChR, acetylcholine receptor; BTX, bungarotoxin; cKO, conditional knockout; DGC, dystrophin-glycoprotein complex; EBS, epidermolysis bullosa simplex; FL, forelimb; HL, hindlimb; IF, intermediate filament; IFBD, intermediate filament–binding domain; Ins16, 16–base pair insertion mutation; MT, microtubule; MyS, myasthenic syndrome; NMJ, neuromuscular junction; OA, okadaic acid; P1, plectin isoform 1; P1b, plectin isoform 1b; P1c, plectin isoform 1c; P1d, plectin isoform 1d; P1f, plectin isoform 1f; VGSC, voltage-gated sodium channel; WFA, withaferin A; wt, wild type.

INTRODUCTION

Mature neuromuscular junctions (NMJs) are highly specialized and complex structures in which postsynaptic acetylcholine receptors (AChRs) are densely packed and precisely aligned across motor-nerve terminals. Considering the heavy use of NMJs and their constant exposure to mechanical stress, the orderly assembly of AChRs into dense clusters during synaptic development as well as their stabilization throughout the life span is critical for proper muscle function. At their cytoplasmic interphase, AChRs are directly bound to rapsyn, a peripheral membrane protein that interacts with multiple synaptic proteins, leading to the clustering of AChRs and their linkage to the underlying cytoskeleton (Wu *et al.*, 2010). Tight regulation of the actin and microtubule (MT) networks has been shown to play a role in vesicular trafficking of AChRs to the postsynaptic

membrane (Lee *et al.*, 2009; Schmidt *et al.*, 2012), AChR movement, and formation of clusters (Dai *et al.*, 2000). In contrast, not much is known about the molecular mechanisms that lead to the stabilization of NMJs and protect them against disassembly.

Previous studies showed that desmin intermediate filaments (IFs) are enriched in the postsynaptic domain of NMJs (Burden, 1982; Sealock *et al.*, 1989; Mitsui *et al.*, 2000). IFs are highly elastic, much more flexible, and less dynamic than actin filaments or MTs (Mucke *et al.*, 2004; Kreplak *et al.*, 2008), and they exhibit stiffening properties when subjected to mechanical stress (Janmey *et al.*, 1991). Postsynaptic IF networks would thus be optimally suited to serve as a physical link between endplates and the contractile apparatus and to provide the structural backbone required for preservation of sarcolemmal infolding, positioning of myonuclei and mitochondria, and stable anchorage of the AChR complex during fiber deformation caused by muscle contraction or regeneration of damaged muscle. In fact, abortive muscle regeneration and modifications in synaptic structure have been reported for desmin-knockout mice (Agbulut *et al.*, 2001). However, the molecular mechanisms underlying the targeting, spatial networking, and specific functions of postsynaptic IFs remained elusive.

Studies on various cell types, among them skeletal muscle fibers, showed that plectin, a >500-kDa, IF-associated cytolinker protein, plays a dominant role in determining IF network architecture and can act also as regulator of IF assembly (Castañón *et al.*, 2013). Plectin's uniqueness as IF network organizer is based on two important molecular features—a universal high-affinity binding site for IF proteins residing in its C-terminal domain and a variable N-terminal sequence preceding a highly conserved actin-binding domain (ABD; Fuchs *et al.*, 1999). The different N-terminal sequences modify the binding specificity of plectin's N-terminus in such a way that different plectin isoforms are targeted to distinct cellular sites. By recruiting IFs via their C-termini to these sites, the different isoforms profoundly affect IF networking and cytoarchitecture (Wiche and Winter, 2011). On this basis, plectin could play a major role in connecting IFs to the NMJ domain of muscle fibers. Moreover, some patients with epidermolysis bullosa simplex with muscular dystrophy (EBS-MD), the most common forms of plectinopathies (Winter and Wiche, 2013), also suffer from myasthenic syndrome (MyS). EBS-MD-MyS manifests as severe deterioration of endplate morphologies, defects in neuromuscular transmission, and progressive limb muscle weakness (Banwell *et al.*, 1999; Forrest *et al.*, 2010; Maselli *et al.*, 2010; Selcen *et al.*, 2011); for review see Engel, 2012.

Studies of patients suffering from EBS-MD with MyS yielded important insights into the development of the disease but did not provide an opportunity to study mechanisms of endplate degeneration on cellular and molecular levels. The generation of plectin-deficient immortalized myoblast cell lines that mimic the pathology of EBS-MD (Winter *et al.*, 2014) offered a unique opportunity to overcome these limitations. We used this tool to investigate whether 1) agrin-induced AChR clustering is affected by plectin deficiency, 2) plectin recruits desmin IFs to AChR complexes, 3) AChR coupling to IFs affects the diffusional mobility of AChRs within the sarcolemma and/or the formation and maintenance of stable clusters, 4) phenotypic alterations effected by plectin deficiency can be rescued by forced expression of specific plectin isoforms, and 5) plectin interacts directly with endplate constituent proteins and, if so, in an isoform-specific manner. To investigate the effect of plectin deficiency on NMJ integrity on the organismal level, we additionally generated a conditional plectin-knockout mouse line (Pax7-Cre/conditional knockout [cKO]) that enables deletion of the plectin gene in skeletal muscle precursor (satellite) cells. Our study demonstrates that plectin mediates the linkage of AChR complexes to the desmin IF network in an isoform-dependent manner and that this linkage is crucial for endplate integrity and proper body locomotion.

RESULTS

Agrin-induced AChR clustering is diminished in the absence of plectin

To study the molecular mechanism behind plectin's contribution to NMJ integrity, we first investigated cluster formation of AChRs in myotubes that had been differentiated ex vivo from immortalized plectin-positive (*Plec*$^{+/+}$) and plectin-deficient (*Plec*$^{-/-}$) myoblast cell lines (Winter *et al.*, 2014). Plectin-deficient myotubes, like their normal counterparts, are multinucleated and show signs of full differentiation, such as spontaneous contraction (Winter *et al.*, 2014). In addition, *Plec*$^{-/-}$ myotubes closely mimic the pathology of EBS-MD myofibers, including the development of desmin-positive protein aggregates (Winter *et al.*, 2014). To induce AChR clustering, myotubes were exposed to recombinant neural agrin, and AChRs were visualized by Alexa 488–α-bungarotoxin (BTX) labeling (Figure 1A). A morphometric analysis revealed that in plectin-deficient myotubes, the formation of large clusters (≥5 μm^2 in size) was strikingly reduced compared to wild-type (wt) cells (Figure 1C). Moreover, such clusters showed reduced fluorescence intensity compared with corresponding ones in plectin-positive myotubes (Figure 1B). On the other hand, in plectin-deficient myotubes, we observed a significantly increased number of (micro) clusters of sizes <5 μm^2 (Figure 1D). To test the responsiveness of *Plec*$^{-/-}$ myotubes to agrin-induced AChR-clustering, we quantified large clusters at different time points after initiating the treatment. In contrast to *Plec*$^{+/+}$ myotubes, where the number of AChR clusters increased consistently with time (Figure 1E), no increase was observed in *Plec*$^{-/-}$ myotubes. In control experiments in which AChR expression levels in myoblasts and myotubes were assessed by immunoblotting, no differences were observed between *Plec*$^{+/+}$ and *Plec*$^{-/-}$ cells, regardless of whether or not they had been treated with agrin (Supplemental Figure S1).

Because AChRs are believed to be incorporated into stable clusters through their linkage to the postsynaptic cytoskeleton (Borges and Ferns, 2001), we investigated whether plectin strengthens such a linkage. For this purpose, we performed a sequential extraction of myotubes (treated or untreated with agrin) with solutions containing increasing concentrations of Triton X-100 (0.01, 0.3, 0.1, and 1%). From each extract, AChRs were precipitated using biotinylated α-BTX and quantified by immunoblotting (Figure 1, F and G). We found that in cells untreated with agrin, the majority of receptors (69.1 and 78.9% in *Plec*$^{+/+}$ and *Plec*$^{-/-}$ cells, respectively) were already solubilized in the combined first two extractions (0.01 and 0.03%; Figure 1, F and G). On treatment with agrin, the amount of receptors extracted at low concentrations of detergent (0.01 and 0.03%) was reduced in plectin-positive cells (52.8%) but not in plectin-deficient cells (83.4%), suggesting that agrin effected a strengthening of the AChR linkage to the underlying cytoskeleton in *Plec*$^{+/+}$ but not in *Plec*$^{-/-}$ myotubes. The proportions of receptors that were extractable only at the higher concentrations of Triton X-100 (0.1 and 1%) were larger (particularly upon agrin treatment) in *Plec*$^{+/+}$ than in *Plec*$^{-/-}$ myotubes (47.2 vs. 16.6%, respectively), indicating a tighter association of the receptors with the underlying cytoskeleton in the presence of plectin (Figure 1, F and G).

Plectin-promoted AChR clustering is accompanied by desmin IF network anchorage

To investigate whether the observed weaker association of AChR complexes with the underlying cytoskeleton in plectin-deficient

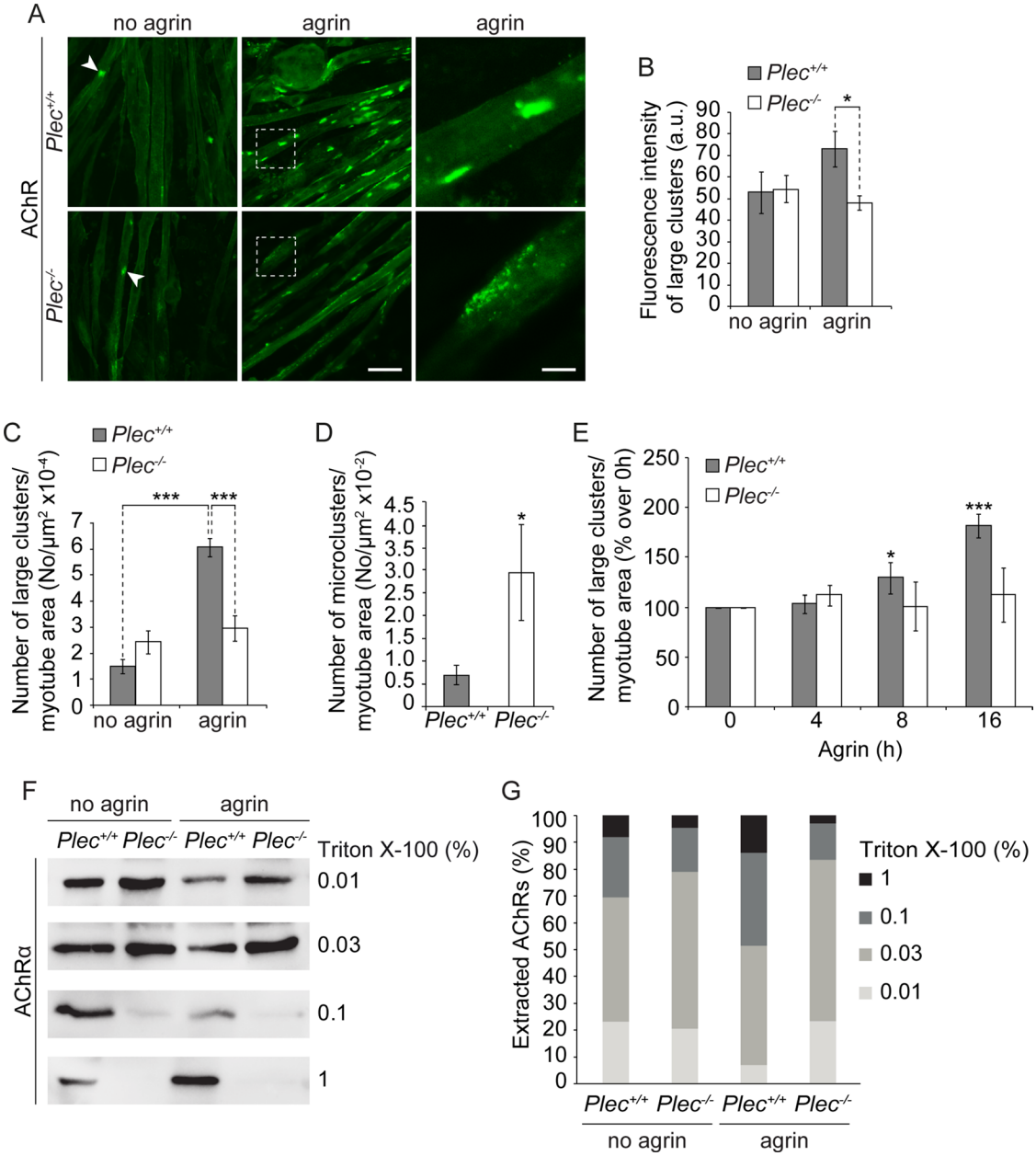

FIGURE 1: Analysis of cluster formation and detergent extractability of AChRs. (A) Representative images of Alexa 488–α-BTX–labeled AChR clusters forming spontaneously (no agrin; white arrowheads) or in the presence of agrin. Right, higher magnification of boxed regions in middle. Note that fragmented and less compact clusters (typical of plectin-deficient cells) are rarely seen in *Plec*$^{+/+}$ cells. Bars, 30 µm (left and middle); 10 µm (right). (B) Statistically evaluated fluorescence intensities (recorded bellow fluorescence saturation) of large (≥5 µm^2) clusters. *Plec*$^{+/+}$, $n = 114$; *Plec*$^{-/-}$, $n = 218$ clusters examined. (C, D) Quantification of large (C) and small (<5 µm^2; micro, D) clusters per total myotube area visualized. Myotubes analyzed: *Plec*$^{+/+}$, 271, and *Plec*$^{-/-}$, 357 (C); and *Plec*$^{+/+}$, 57, and *Plec*$^{-/-}$, 38 (D). Note that upon agrin treatment, *Plec*$^{-/-}$ myotubes form approximately half as many (and ~1.3-fold less dense) large clusters compared with *Plec*$^{+/+}$ cells. (E) Quantification of agrin-induced clusters at different time points (presented as percentage increase over 0 h). Note that only *Plec*$^{+/+}$ cells were responsive to agrin. Myotubes analyzed per time point: *Plec*$^{+/+}$, ≥200; *Plec*$^{-/-}$, ≥203. (F) Immunoblotting (using antibodies to AChR subunit α) of affinity-purified (biotin–α-BTX) AChRs after sequential extraction of *Plec*$^{+/+}$ and *Plec*$^{-/-}$ myotubes with indicated concentrations of Triton X-100. (G) Bar diagram showing proportional extractability (%) of AChRs at various concentrations of detergent. Mean ± SEM, three experiments (B–E), five experiments (G), each. *$p < 0.05$ and ***$p < 0.001$ compared with *Plec*$^{+/+}$ (D) or *Plec*$^{+/+}$ agrin/no agrin/0 h (B, C ,E). Unpaired Student's *t* test.

myotubes was due to the detachment of desmin IFs and/or actin from the complexes, we performed costainings of *Plec*$^{-/-}$ and *Plec*$^{+/+}$ myotubes, using Alexa 488–α-BTX for visualization of AChRs and antibodies to either desmin or actin. Confocal imaging revealed dense desmin IF networks juxtaposed to the AChRs in *Plec*$^{+/+}$ myotubes, whereas in plectin-deficient myotubes, desmin IFs were detached from the AChR clusters and collapsed into massive aggregates (Figure 2A). In contrast, plectin-positive and -negative myotubes showed no differences in AChR association with the actin network (Figure 2A). To assess in a more direct way whether the

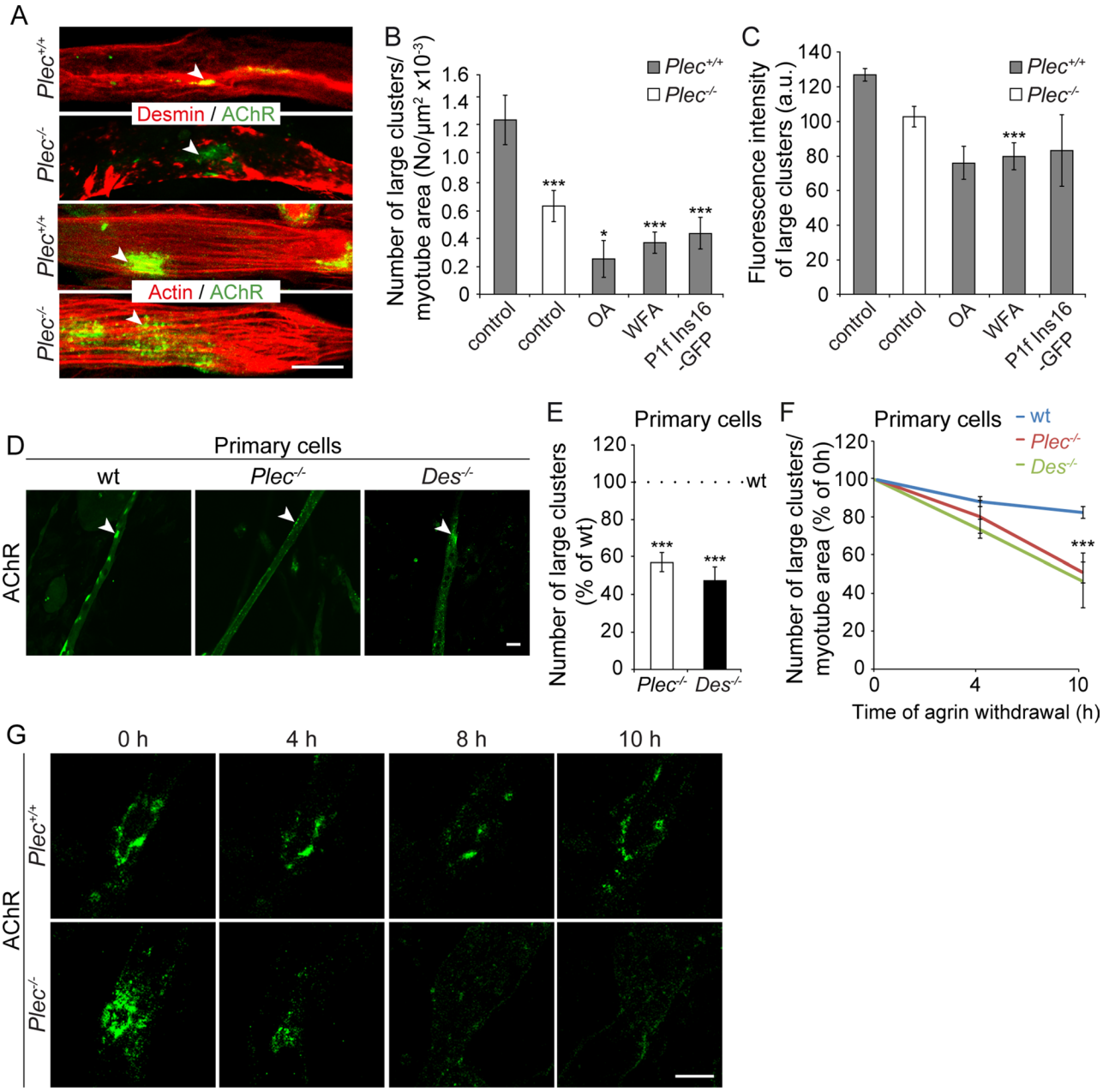

FIGURE 2: Compromised AChR clustering in myotubes deficient in plectin or desmin. (A) Confocal images of *Plec*$^{+/+}$ and *Plec*$^{-/-}$ myotubes double labeled for AChR (Alexa 488–α-BTX) and desmin (top) or actin (bottom). Note embedment of AChRs in desmin IF networks in *Plec*$^{+/+}$ cells vs. dispersal of the receptors and separation from aggregated networks in *Plec*$^{-/-}$ myotubes. Note also the association of actin fibers with AChRs in both *Plec*$^{-/-}$ and *Plec*$^{+/+}$ myotubes. (B, C) Quantification of large AChR clusters per myotube area (B) and evaluation of their density (C) upon treatment of *Plec*$^{+/+}$ cells with OA or WFA or after overexpression of P1f-Ins16. Controls, untreated cells. Note the treatment-effected reduction of both assessed parameters to levels even below those of *Plec*$^{-/-}$ myotubes. Myotubes analyzed (B): *Plec*$^{+/+}$, untreated, 188, and treated, 125; *Plec*$^{-/-}$, 64. Clusters analyzed (C): *Plec*$^{+/+}$, untreated, $n = 92$, and treated, $n = 71$; *Plec*$^{-/-}$, 53. (D, E) Representative confocal images of AChR clusters in wt, *Plec*$^{-/-}$, and *Des*$^{-/-}$ myotubes differentiated from primary myoblasts (D) and numerical evaluation of AChR clusters per myotube area (E). Myotubes analyzed: wt, 406; *Plec*$^{-/-}$, 183; and *Des*$^{-/-}$, 333. (F) AChR clusters quantified at different time points after withdrawal of agrin from myotubes specified in D. Values at 0 h after withdrawal of agrin were set as 100%. Myotubes examined: $n \geq 26$ per genotype at each time point. Mean ± SEM, three experiments each. *$p < 0.05$ and ***$p < 0.001$ compared to *Plec*$^{+/+}$ (B, C), or wt (E, F). Unpaired Student's *t* test (B, C), or one-way ANOVA (E, F). (G) Time-lapse images of Alexa 488–α-BTX–labeled AChR clusters at indicated time points after withdrawal of agrin. Bars, 20 µm (A, top; D), 10 µm (A, bottom; G).

association of IF network with AChRs had an effect on the formation and/or stability of clusters, we monitored agrin-induced clustering after disruption of desmin IF networks in immortalized *Plec*$^{+/+}$ myotubes using okadaic acid (OA). OA, a potent phosphatase inhibitor, was previously shown to cause IF collapse in a number of cell types, including fibroblasts (Gregor *et al.*, 2014) and keratinocytes (Strnad *et al.*, 2002; Osmanagic-Myers *et al.*, 2006). As shown in Figure 2, B and C, OA treatment of *Plec*$^{+/+}$ myotubes led to a dramatic

reduction in the number and density of agrin-induced clusters to levels even below those of plectin-deficient myotubes. To establish that OA-effected abnormal clustering was directly linked to IF retraction from the receptors and did not represent just a secondary effect of OA-induced hyperphosphorylation, we investigated receptor clustering upon treatment with withaferin A (WFA), a small molecule that covalently modifies the highly conserved α-helical coiled-coil 2B domain of type III IFs, leading to their aggregation in vitro and in vivo (Bargagna-Mohan *et al.*, 2007). As shown in Figure 2, B and C, WFA affected AChR clustering in a way very similar to OA. Furthermore, to directly interfere with plectin's IF-anchoring function, we transfected into *Plec*$^{+/+}$ myoblasts a cDNA expression plasmid encoding a defective plectin (plectin isoform 1f [P1f]–16-base pair insertion mutation [Ins16]) that carried a mutation near its IF-binding domain (IFBD); this mutation had previously been found to cause a human plectinopathy characterized by a severely disorganized desmin filament network (Schröder *et al.*, 2002). The analysis of myotubes derived from such cells clearly revealed a retraction of the desmin IF network from the periphery of the cell and its collapse in interior regions (unpublished data). A quantitative analysis revealed a numerical reduction (Figure 2B), as well as a diminished density, of AChR clusters (Figure 2C). Overall the effects of all these treatments (OA, WFA, and forced expression of mutant plectin) on AChR clustering were quantitatively very similar, strongly suggesting that IF network collapse was indeed responsible for the diminished frequency and density of the receptor clusters (Figure 2, B and C).

To assess whether plectin and desmin deficiencies affected AChR clustering in similar ways, we directly compared agrin-induced AChR cluster formation in myotubes generated by differentiation of either *Plec*$^{-/-}$ or *Des*$^{-/-}$ primary myoblasts (Figure 2, D and E). In both cases, we observed a striking reduction in the number of agrin-induced clusters per myotube area (54.5 and 47.6% of wt levels, respectively), comparable to the levels measured for immortalized myocytes (Figure 1C).

To further verify the role of plectin and desmin as stabilizers of AChR clusters, we quantified the number of AChR clusters remaining in wt, *Plec*$^{-/-}$, and *Des*$^{-/-}$ myotubes after withdrawal of agrin. As shown in Figure 2F, after 4 h of incubation in agrin-free medium, the number of detectable clusters had declined in all cases. However, in *Plec*$^{-/-}$ and *Des*$^{-/-}$ myotubes, the decline (19 and 25%, respectively) was about twice as fast as in their wt counterpart (11%). After 10 h, the number of clusters in *Plec*$^{-/-}$ and *Des*$^{-/-}$ myoblasts had dropped to 48 and 52%, respectively, whereas in wt cells, it showed a decline of only 16% (Figure 2F). Time-lapse live imaging (at 2-h intervals up to 10 h after agrin withdrawal) of Alexa 488–α-BTX–labeled AChR clusters in immortalized myoblast-derived *Plec*$^{-/-}$ and *Plec*$^{+/+}$ myotubes confirmed the rapid degradation of clusters in plectin-deficient cells, whereas the vast majority of clusters in *Plec*$^{+/+}$ myotubes appeared to be stable up to the 10-h time point (Figure 2G). Hence desmin-deficient myotubes phenotypically closely resembled their plectin-deficient counterparts, suggesting that the loss of filaments as a whole and the disruption of their anchorage due to plectin deficiency affected AChR clustering in similar ways.

Increased diffusional mobility of AChRs within the sarcolemma of plectin-deficient myotubes

To visualize the dynamic interplay of AChR clusters and IFs, we performed live imaging of desmin–green fluorescent protein (GFP)–transfected *Plec*$^{+/+}$ and *Plec*$^{-/-}$ myotubes that after withdrawal of agrin were additionally labeled with Rhodamine Red–streptavidin-biotin-α-BTX. Monitoring *Plec*$^{+/+}$ cells for up to 2 h in the absence of agrin, we observed compact and relatively immobile AChR clusters enclosed in a lattice of desmin IFs (Figure 3A and Supplemental Video S1). In contrast, in *Plec*$^{-/-}$ myotubes, collapsed desmin IF networks were visualized as aggregates that were distant from receptor clusters without showing any overlap. Of interest, already as early as 6 min after initiating the imaging period, fragmentation and a drifting away from IF-disconnected larger clusters could be observed in this case (Figure 3B and Supplemental Video S2). Moreover, large clusters as a whole were changing their position within the plane of the sarcolemma (Figure 3B and Supplemental Video S2). Finally, transient and apparently unstable interactions between microclusters were detected, suggesting that these structures were unable to fuse into more stable larger clusters (Figure 3B and Supplemental Video S2). When agrin-induced AChR cluster formation was monitored by live imaging of transfected GFP-AChR-ε-subunit instead of α-BTX labeling, similar results were obtained (Supplemental Videos S5 and S6).

Measuring the number of mobile microclusters per visualized myotube area, we found a strikingly higher number in *Plec*$^{-/-}$ than in *Plec*$^{+/+}$ cells (Figure 3C). Not only were the clusters in plectin-deficient myotubes traveling over longer distances, but they also moved with higher velocity than their counterparts in normal cells (Figure 3, D and E). To assess whether desmin IF disruption in *Plec*$^{+/+}$ myotubes led to a phenotype resembling that of *Plec*$^{-/-}$ cells, we exposed plectin-positive myotubes to either OA or WFA or transfected them with P1f-Ins16 (Supplemental Video S3). These manipulations led not only to the expected disruption of desmin IF networks and their detachment from receptor clusters, but also to an increase in number, average velocities, and total distances traveled of mobile clusters, approaching or even exceeding the values measured for *Plec*$^{-/-}$ cells (Figure 3, C–E).

Plectin isoform–specific rescue of compromised AChR clustering and IF network anchorage

Double labeling of soleus muscle fibers for plectin and presynaptic (synaptophysin) or postsynaptic (AChR) marker proteins, using specific antibodies (plectin and synaptophysin) and Alexa 488–α-BTX for visualization of AChRs, revealed extensive overlap of plectin-specific signals with the postsynaptic marker (Supplemental Figure S2A). To identify the NMJ-associated isoform(s) of plectin, we performed double labeling of adult wt myofibers using Alexa 488–α-BTX in combination with specific antibodies to plectin isoform 1 (P1) and P1f, both of which had previously been shown to reside predominantly in peripheral areas of myofibers (Rezniczek *et al.*, 2007; Hijikata *et al.*, 2008; Konieczny *et al.*, 2008). As shown in Supplemental Figure S2B, P1f showed conspicuous codistribution with AChRs, whereas anti-P1 antibodies, in agreement with previous studies (Rezniczek *et al.*, 2007), decorated predominantly structures in the vicinity of synaptic nuclei, in fact generating a negative image of Alexa 488–α-BTX–positive structures.

To assess whether AChR cluster formation and stabilization in cells were directly linked to plectin and especially to P1f, the isoform specifically associated with NMJs (Supplemental Figure S2B), we performed rescue experiments in which *Plec*$^{-/-}$ myoblasts were transiently transfected with cDNA expression plasmids encoding fusion proteins of GFP and various intact and mutated isoforms of plectin. We found that after transfection of P1f-GFP expression plasmids into myoblasts and their differentiation to myotubes, not only was P1f-GFP primarily localized at the sarcolemma of the cells, showing a specific enrichment at AChR clusters (Figure 4A), but, remarkably, it also reestablished desmin IF network association with the receptors (Figure 4A). A quantitative analysis revealed that the number of AChR clusters was significantly increased compared with nontransfected

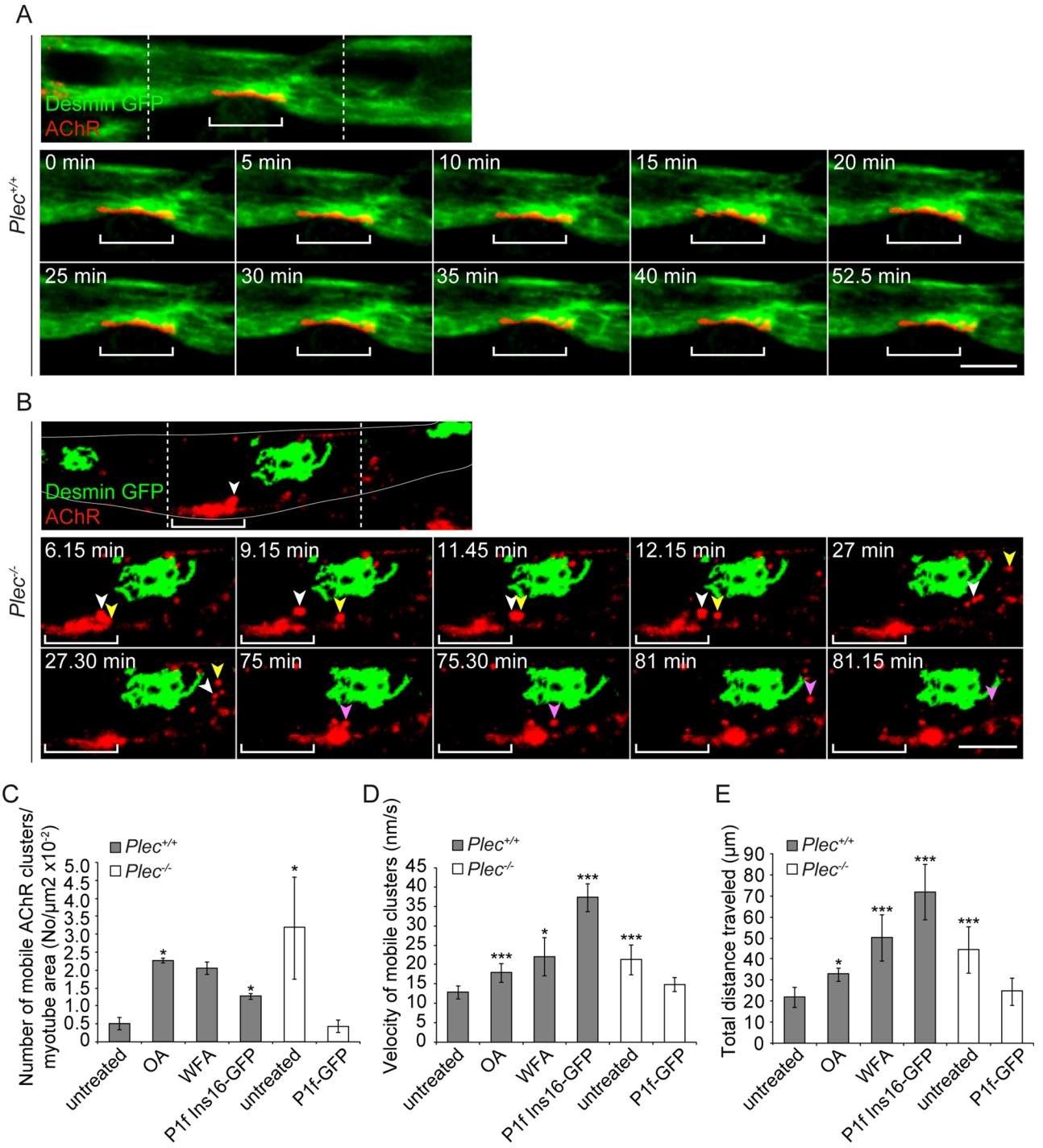

FIGURE 3: Time-lapse video microscopy of desmin-GFP–expressing *Plec*$^{+/+}$ and *Plec*$^{-/-}$ myotubes. (A) Top, confocal image showing part of a desmin-GFP–expressing *Plec*$^{+/+}$ myotube; Rows below, time-lapse images of the central area (delineated by dashed lines). Bracket indicates region of a representative large AChR cluster embedded in a dense network of desmin IFs. Note the nearly unchanged position and compactness of AChR cluster over the entire observation period (0–52.5 min; see also Supplemental Video S1). (B) As in A, except that a *Plec*$^{-/-}$ myotube is shown. Cell margins are outlined in white. Note the prominent desmin IF network aggregate, distant from clusters. White and yellow arrowheads, microclusters separating from a large cluster; note their repeated transient mutual interaction during traveling and final disassembly of the one labeled white in three even smaller microclusters. Purple arrowhead, separation of another microcluster (magenta; time point 75 min) that drifts away and eventually vanishes completely (see also Supplemental Video S2). Note also positional shift of the large cluster as a whole relative to its initial position (bracket). Bars, 10 µm (A, B). (C–E) Statistical quantification of mobile cluster parameters (number, velocity, and total distance traveled) in *Plec*$^{+/+}$ cells (before or after induction of IF network collapse using OA, WFA, or P1f-Ins16) and in unreconstituted or P1f-reconstituted *Plec*$^{-/-}$ cells. Myotubes analyzed in C: *Plec*$^{+/+}$, untreated, 6, and treated, 7; *Plec*$^{-/-}$, 5; and P1f-GFP, 5. Clusters analyzed in D and E: *Plec*$^{+/+}$, untreated, 202, and treated, 174; *Plec*$^{-/-}$, 217; and P1f-GFP, 21. Mean ± SEM, three independent experiments. *$p < 0.05$ and ***$p < 0.001$ compared with *Plec*$^{+/+}$, untreated; unpaired Student's *t* test.

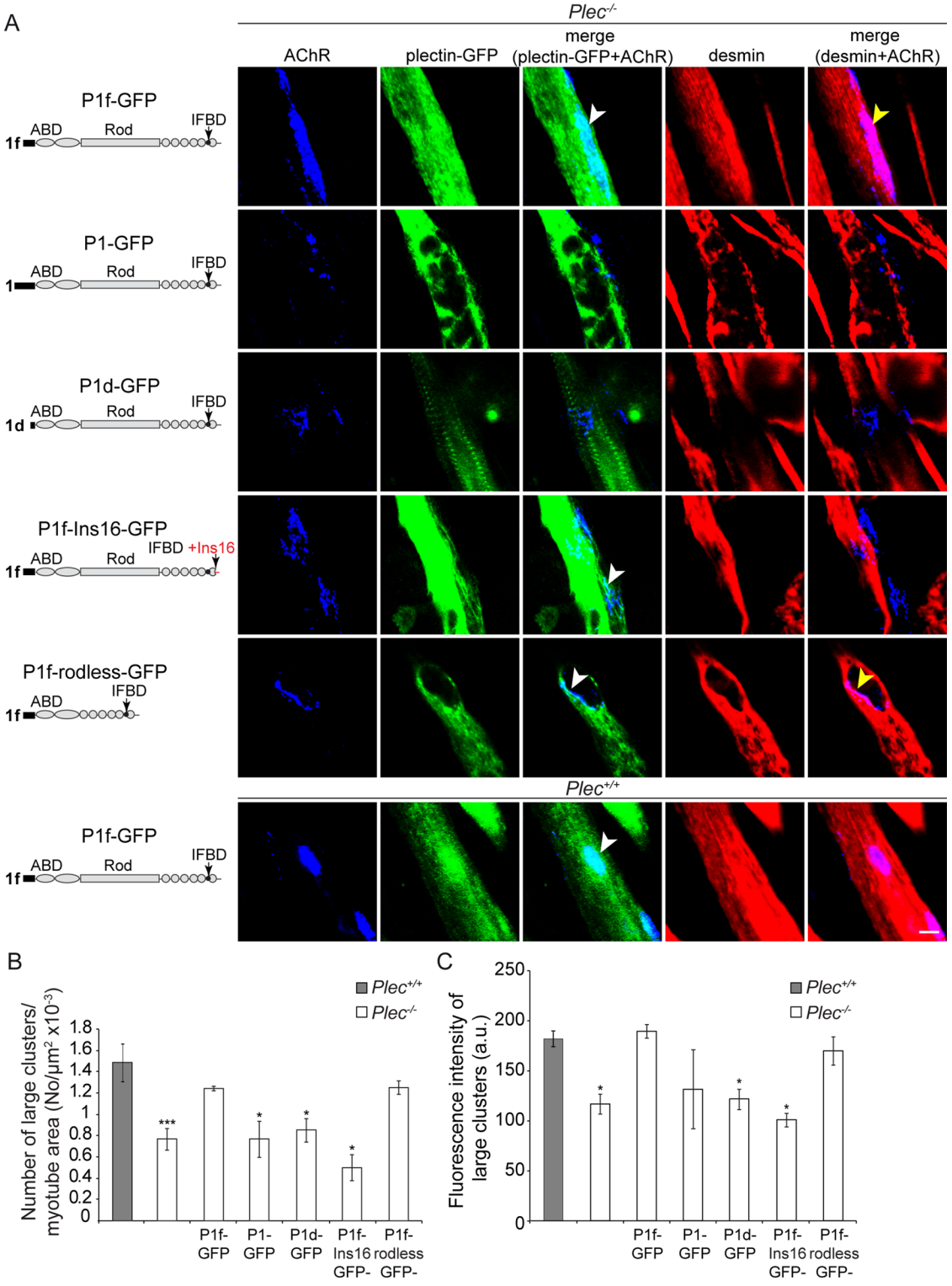

FIGURE 4: Plectin-isoform dependent rescue of compromised AChR clustering and IF anchorage in plectin-deficient myotubes. (A) Confocal fluorescence images of *Plec*$^{-/-}$ (top five rows) and *Plec*$^{+/+}$ (bottom row) myotubes after transfection with plasmids encoding various intact or mutant versions of plectin-GFP fusion proteins. Schematic drawings of plectin variants precede each row. Single- and two-channel images (merged) of triple-labeled specimens are presented as indicated on top. Note that among three different isoforms of plectin tested, only P1f showed targeting to AChR complexes (white arrowheads in the top and two lower rows), whereas recruitment of desmin IFs toward receptor complex was dependent on P1f comprising an intact IFBD (yellow arrowheads). Bar, 10 μm. (B, C) Quantification of numbers (B) and densities (C) of large AChR clusters measured in three independent experiments for each series of transfections. Note that only full-length or rodless P1f could restore compact receptor clusters. Myotubes analyzed in B: *Plec*$^{+/+}$, 359; *Plec*$^{-/-}$, untransfected, 727, and transfected 536. Clusters examined in C: *Plec*$^{+/+}$, 273; *Plec*$^{-/-}$, untransfected, 530, and transfected, 758. Mean ± SEM. *$p < 0.05$ and ***$p < 0.001$ compared with *Plec*$^{+/+}$; unpaired Student's *t* test.

Plec$^{-/-}$ myotubes, approaching the level detected in plectin-positive myotubes (Figure 4B). In contrast, when nuclear/ER membrane–associated isoform P1 (P1-GFP) and Z-disk–associated isoform P1d (P1d-GFP) were expressed, neither of them colocalized with the receptor complex, nor did they reestablish desmin IF network accumulation in defined sarcolemmal areas, indicating that they failed to promote AChR cluster formation (Figure 4, A and B). Similarly, when the experiments were performed with plasmids encoding IF-binding–incompetent P1f (P1f-Ins16), neither reanchoring of IF networks at AChR clusters nor improved receptor clustering was observed in myotubes (Figure 4, A and B). On the other hand, a significant increase in the number of AChR clusters, paralleled by desmin reanchorage, was observed upon forced expression of P1f-rodless, a P1f version lacking the rod but containing the other domains of the plectin molecule, including its IFBD (Figure 4, A and B). Codistribution of P1f with AChR clusters was observed also upon its overexpression in wt myotubes (Figure 4A). When the compactness of receptor clusters in P1f-reconstituted versus unreconstituted myotubes was evaluated by quantifying the fluorescence intensities of Cy5–α-BTX–labeled clusters, only the expression constructs that encoded full-length or rodless P1f were found to effect the formation of more compact receptor clusters, whereas those encoding isoforms P1 or P1d or P1f-Ins16 were not (Figure 4C).

Furthermore, using video microscopy, we showed that the elevated mobility of clusters in *Plec*$^{-/-}$ myotubes could be restored to the lower levels typical of plectin-positive myotubes (Figure 3, C–E, and Supplemental Video S4). These observations confirmed that P1f-mediated IF anchorage of AChRs decreased their mobility and counteracted the formation of reassembly-incompetent microclusters.

Targeting of plectin to the AChR complex is accomplished by interaction of its ABD with rapsyn

To study P1f's interaction with the AChR complex on the molecular level, we selectively isolated sarcolemma-associated AChRs from C2C12 myotubes by incubating live cells with biotinylated α-BTX and purifying bound receptors after cell lysis with streptavidin-agarose (Borges and Ferns, 2001). Among the proteins copurifying with the receptor, P1f could unambiguously be identified by immunoblotting using isoform-specific antibodies (Figure 5A). Of interest, P1f copurified with the AChR complex at levels higher than background only when myotubes had been treated with agrin, suggesting that this was inducing P1f-AChR complex formation.

To examine whether P1f could interact with AChR complex–specific proteins that potentially could be involved in its targeting to NMJs, we tested its interaction with the AChR-binding protein rapsyn. On immunoprecipitation of rapsyn from C2C12 myotube lysates, endogenous P1f was one of the coprecipitating proteins (Figure 5B). Moreover, this interaction was agrin dependent, as greater than four times higher levels of P1f were coprecipitating from lysates of agrin-treated versus untreated myotubes (Figure 5B).

To assess whether plectin's isoform diversity played a role in rapsyn-binding, we expressed and purified recombinant histidine (His)-tagged versions of N-terminal fragments of isoforms P1f and P1d (each comprising the isoform-specific, first exon–encoded sequence and ABD encoded by the ensuing exons 2–8), as well as of the ABD alone (without any preceding isoform-specific sequences; Figure 5E, boxed area) and performed a pull-down assay in which the binding of these proteins to a GST-rapsyn fusion protein immobilized on Sepharose beads was tested. Immunoblotting of bound (eluates) and unbound fractions revealed rapsyn binding of P1f-ABD, as well as of the ABD without preceding sequences (Figure 5C, top two rows, lanes 4 and 5), whereas P1d-ABD showed hardly any binding (Figure 5C, top two rows, lane 6 vs. lane 9). Control experiments in which Sepharose beads coupled to glutathione *S*-transferase (GST) instead of rapsyn-GST or uncoupled beads were used were negative (Figure 5C, bottom four rows).

In an alternative assay, HEK cells were cotransfected with expression plasmids for rapsyn-hemagglutinin (HA) and GFP-tagged versions of N-terminal plectin fragments, followed by HA-specific immunoprecipitation and analysis of rapsyn-bound proteins by immunoblotting using antibodies to GFP/HA tags. In this case, too, P1f-ABD and ABD showed specific binding to rapsyn, whereas P1d-ABD did not (Figure 5D, top two rows, lanes 4-6); control experiments with HEK cells transfected with expression plasmids solely for plectin fragments but not for rapsyn-HA were negative (Figure 5D, bottom two rows). Overall these data suggested that exon 1f–encoded, but not P1d-specific, amino acid residues favored plectin's interaction with rapsyn.

Plectin deficiency causes NMJ deterioration and reduction in AChR density in Pax7-Cre conditional knockout mice

The inefficient AChR clustering observed in ex vivo–differentiated plectin-deficient myotubes, together with the grossly disorganized structure of NMJs typical for patients suffering from plectinopathy-associated MyS (Engel, 2012), strongly suggested that postsynaptic plectin plays a role in maintaining dense AChR clusters at the crests of sarcolemma infoldings. To examine on the organismal level whether the lack of postsynaptic plectin causes defects in NMJ morphology with consequences for muscle strength and body balance, we generated a mouse line (Pax7-Cre/cKO) in which plectin gene disruption was controlled by Pax7, a transcription factor that is expressed in muscle stem cells (Relaix *et al.*, 2005). In contrast to a previously generated MCK-Cre/cKO mouse line (Konieczny *et al.*, 2008), in which precursor satellite cells were exempt from ablation (allowing reexpression of plectin in adult myofibers during regeneration), Pax7-Cre/cKO mice were plectin negative not only in mature myofibers of limb muscles, but also in satellite cells (Supplemental Figure S3) and consequently at NMJs (Figure 6A). Whereas MCK-Cre/cKO mice were hardly distinguishable from their wt littermates until reaching adulthood, Pax7-Cre/cKO mice suffered from body weakness, manifesting as small size, profound kyphosis, and a survival rate of only 50% at the age of 19 wk (Figure 6, B and C).

To distinguish between presynaptic and postsynaptic contributions of plectin to the structural integrity of NMJs, we compared morphological features of NMJs in specimens isolated from wt and four different genetically modified mouse lines, namely Pax7-Cre/cKO, MCK-Cre cKO (Konieczny *et al.*, 2008), desmin-knockout (*Des*$^{-/-}$) mice (Li *et al.*, 1996), and mice deficient in plectin isoform 1c (P1c), the major isoform expressed in motor neurons (Fuchs *et al.*, 2009). Of interest, in soleus muscle of adult Pax7-Cre/cKO mice, we observed a dramatic deterioration of endplates into small islands of AChRs, in sharp contrast to the continuous (pretzel-like) appearance of AChR clusters in wt as well as in P1c-knockout mice (Figure 7A). The quantification of Alexa 488– α-BTX–specific signals in Pax7-Cre/cKO soleus muscle revealed a decrement of 51% compared to wt, suggesting a substantial reduction of AChR density in the absence of plectin (Figure 7B). Deterioration of the typical pretzel-like appearance was noticeable also in *Des*$^{-/-}$ and MCK-Cre/cKO mice, albeit in both of these cases it was less pronounced, as clearly revealed by statistical quantification of the number and sizes of fragmented clusters (Figure 7, C and D). Apart from soleus, severe fragmentation of NMJs was found in several other types of

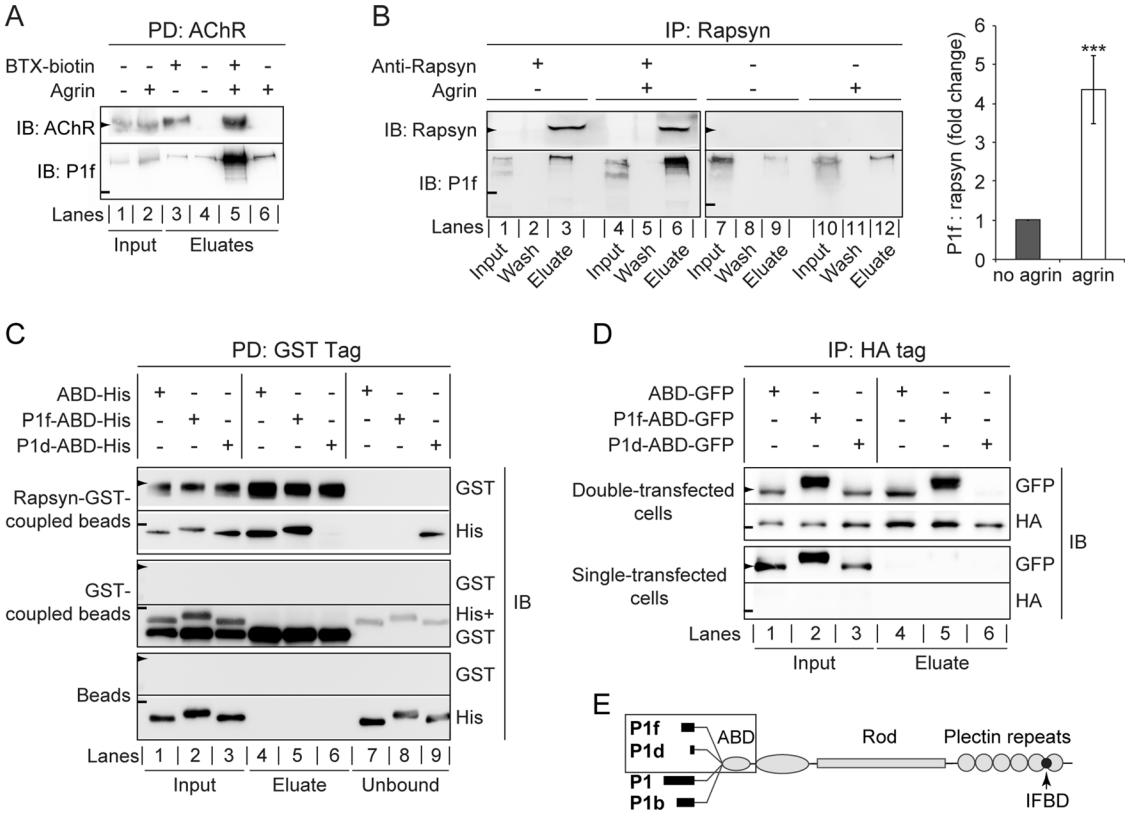

FIGURE 5: Targeting of P1f to the AChR complex via binding to rapsyn. (A) Copurification of P1f with sarcolemma-associated AChRs. Membrane-bound AChRs were isolated from untreated or agrin-treated C2C12 myotubes by incubation of cells with biotinylated α-BTX, followed by cell lysis and precipitation of the biotinylated AChR using streptavidin-agarose. Input (lysates) and eluate fractions were analyzed by immunoblotting (IB). Lysates from BTX-untreated cells served as negative controls (lanes 4 and 6). (B) Coimmunoprecipitation of P1f with rapsyn from lysates of untreated/agrin-treated C2C12 myotubes (input) using anti-rapsyn antibodies and protein G–agarose. Wash and eluate fractions of precipitates were subjected to immunoblotting (IB) as indicated. Note that the levels of endogenous rapsyn are very low and become detectable only upon immunoprecipitation of the protein. The bar diagram shows signal intensities of P1f, densitometrically determined and normalized to coeluted rapsyn (P1f/rapsyn = 1, for agrin-untreated cells). Note the greater than fourfold higher amount of P1f cosedimenting with rapsyn from agrin-treated C2C12 myotubes compared to control (no agrin). Mean value ± SEM, three experiments. ***$p < 0.001$ compared with no-agrin control. (C) GST pull-down assay. Top two rows, recombinant rapsyn-GST coupled to glutathione–Sepharose beads was incubated with His-tagged versions of plectin's ABD, P1f-ABD, or P1d-ABD, and rapsyn-bound/unbound fractions were separated by centrifugation. Aliquots of input (lanes 1–3), bound (eluates; lanes 4–6), and unbound fractions (lanes 7–9) were analyzed by immunoblotting (IB) using antibodies to protein tags as indicated. Middle two and lower two rows, like the top two rows, except that only recombinant GST protein (without fused rapsyn) or no protein at all, respectively, was immobilized on glutathione–Sepharose beads. Note that P1f-ABD, as well as ABD, is coeluting with rapsyn-GST (second row, lanes 4 and 5), whereas P1d-ABD is predominantly detected in the unbound fraction (lane 9). (D) Pull down of N-terminal plectin fragments with rapsyn overexpressed in HEK cells. Top two rows, lysates derived from HEK-cells cotransfected with rapsyn-HA and GFP-tagged plectin fragments were subjected to immunoprecipitation using HA-specific antibodies and protein G–coupled agarose beads; input and eluate fractions were analyzed as in to D. Note the binding of P1f-ABD and ABD (lanes 4 and 5), but not of P1d-ABD (lane 6), to rapsyn-HA. Bottom two rows, like the upper two rows, except that HEK cells were single transfected (overexpressing plectin fragments but not rapsyn). (E) Schematic representation of the domain structure of the four major plectin isoforms (P1f, P1d, P1, and P1b) expressed in skeletal muscle. Recombinant His/GFP-tagged N-terminal domains of isoforms used for binding assays and coimmunoprecipitation are boxed. Arrowheads and short lines on the left in A–D mark positions of molecular mass markers (in kilodaltons): A and B, 43 and 250; C, 70 and 35; D, 55 and 43 (arrowheads and lines, respectively).

plectin-deficient muscle tested, such as extensor digitorum longus, gastrocnemius, tibialis, and diaphragm (Supplemental Figure S4). Concomitant with the fragmentation of NMJs, a disturbed topology of the nerve terminal was observed (Figure 7F). Moreover, we found a dispersion of voltage-gated sodium channels (VGSCs) in endplate regions of Pax7-Cre/cKO soleus muscle (Figure 7G), manifesting as approximately twofold reduced colocalization of VGSCs with AChRs (Figure 7E).

Monitoring age-dependent progression of NMJ fragmentation in soleus muscle of wt, Pax7-Cre/cKO, and *Des*$^{-/-}$ mice in a comparative manner showed that the frequency of fragmented NMJs (defined here as NMJs with ≥6 discontinuous fragments of AChRs) in 1-mo-old animals already reached 21.2% in Pax7-Cre/cKO versus only 4.1% in corresponding *Des*$^{-/-}$ mice (Figure 7H). At the age of 2 mo, Pax7-Cre/cKO mice displayed a striking deterioration of their endplates (65% fragmented NMJs compared with only 24.4% in

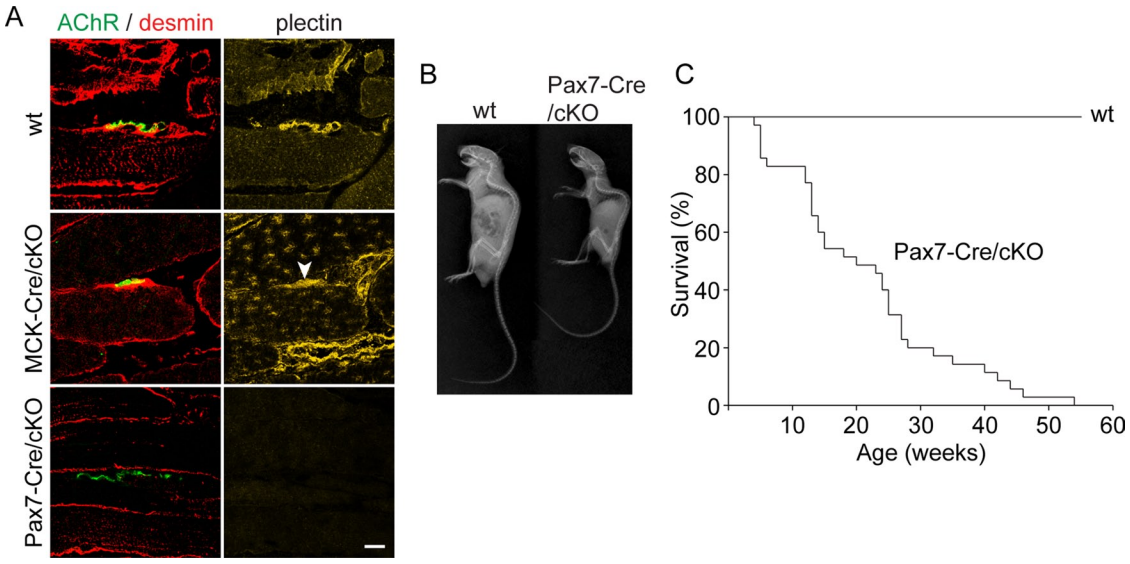

FIGURE 6: Phenotypic characterization of Pax7-Cre/cKO mice. (A) Longitudinal cryosections of soleus muscles derived from adult wt, MCK-Cre/cKO, and Pax7-Cre/cKO mice were immunolabeled for plectin (yellow) and desmin (red) and labeled for AChR with Alexa 488–α-BTX (green). Note the complete absence of plectin from myofibers (including endplate regions) of Pax7-Cre/cKO mice, whereas myofibers from adult MCK-Cre/cKO mice showed some reexpression and accumulation of plectin at endplate regions (arrowhead). (B) X-radiography of wt and Pax7-Cre/cKO mice. Note severe kyphosis in Pax7-Cre/cKO mice. (C) Survival rates of wt and Pax7-Cre/cKO mice. Note greatly reduced lifespan of mutant mice, showing a 50% survival rate of only 19 wk ($n > 35$ per genotype).

Des$^{-/-}$ samples), and after 4 mo, fragmentation had risen to 84.2% in Pax7-Cre/cKO versus 54.5% in *Des*$^{-/-}$ mice (Figure 7H). Thus *Des*$^{-/-}$ mice showed progressive but significantly milder fragmentation of NMJs than plectin-deficient animals (Figure 7H).

To investigate whether plectin deficiency affected the ultrastructure of NMJs, in particular the typical infoldings of the sarcolemma, we subjected epoxy resin–embedded ultrathin sections of soleus muscle from adult wt and Pax7-Cre/cKO mice to electron microscopy. Whereas in wt mice, the postsynaptic region was characterized by numerous, evenly distributed infoldings of uniform depth, in Pax7-Cre/cKO mice, synaptic infoldings were strikingly rare and of uneven shape (Figure 8, A, left and center, and B). In addition, a dearth of postsynaptic mitochondria was noticeable (Figure 8, A, right, and C).

Postsynaptic plectin deficiency causes retraction of IFs from NMJs with ensuing network collapse and accumulation of MT networks at endplates

To investigate whether plectin's association with NMJs led to the accumulation and anchorage of IF networks at the synapses, we performed costaining of AChRs and desmin IFs. Consistent with our observations made with ex vivo–differentiated myotubes (Figure 2A), en face confocal imaging revealed dense desmin IF networks juxtaposed to the NMJ in wt muscle, whereas in Pax7-Cre/cKO muscle, desmin IFs were detached from the synapse and showed collapse around synaptic nuclei (Figure 9A). Three-dimensional reconstructions of confocal *Z*-stack images of muscle fibers costained for desmin, AChRs, and synaptophysin provided clear evidence for the retraction of desmin IFs from NMJs in plectin-deficient muscle (Figure 9B and Supplemental Videos S7 and S8). Similarly, cytokeratins, a second, although in muscle fibers less abundantly expressed IF type (Ursitti *et al.*, 2004), showed accumulation around NMJs in wt but not *Plec*$^{-/-}$ muscle fibers (Figure 9C). Similarly, using antibodies to nestin, an IF protein that is specifically expressed at NMJs and myotendinous junctions of adult skeletal muscle fibers (Carlsson *et al.*, 1999), showed that nestin-positive filaments were separated from the postsynaptic apparatus in plectin-negative fibers (Figure 9D). With the use of vimentin-specific antibodies, in neither wt nor *Plec*$^{-/-}$ soleus muscle fibers were positive filaments observed (Figure 9E).

We recently showed that MT networks in plectin-deficient myotubes, similar to *Plec*$^{-/-}$ keratinocytes, were more stable and thus less dynamic due to their increased association with MT-stabilizing proteins such as tau and MAP2c (Raith *et al.*, 2013; Valencia *et al.*, 2013). As a consequence, several important MT-dependent cellular functions were found to be altered or compromised in plectin-deficient cells, among them vesicular transfer of glucose transporters to the sarcolemma of muscle fibers (Raith *et al.*, 2013). Because previous reports suggested a vectorial delivery of synaptic proteins via stable MT tracks to the synaptic membrane (Marchand *et al.*, 2000; Schmidt *et al.*, 2012), we investigated whether alterations in MT organization contributed to the compromised AChR clustering observed in plectin-deficient myotubes. Double labeling, using Alexa 488–α-BTX and antibodies to tubulin, showed that the MT networks surrounding the IF-deserted AChR complexes in plectin-deficient soleus muscle fibers (Figure 9F), as well as those in cultured myotubes (Supplemental Figure S5A), were indeed more dense and thus more prominent than in wt cells. MTs in plectin-deficient muscle also showed a higher extent of tubulin acetylation (Figure 9F) and more prominent decoration with the MT assembly–promoting protein tau (Figure 9F and Supplemental Figure S5A), both indicators of increased MT polymer stability.

To assess whether the stabilization of MTs in wt myotubes mimics the situation of reduced agrin-inducible AChR clustering typical of plectin-deficient cells, we either treated wt myotubes with Taxol or subjected them to forced expression of tau-GFP before agrin exposure. Both treatments, although leading to a much more prominent peripheral MT network compared with untreated cells, led to reductions in cluster formation to levels even lower than that of *Plec*$^{-/-}$ cells (Supplemental Figure S5B).

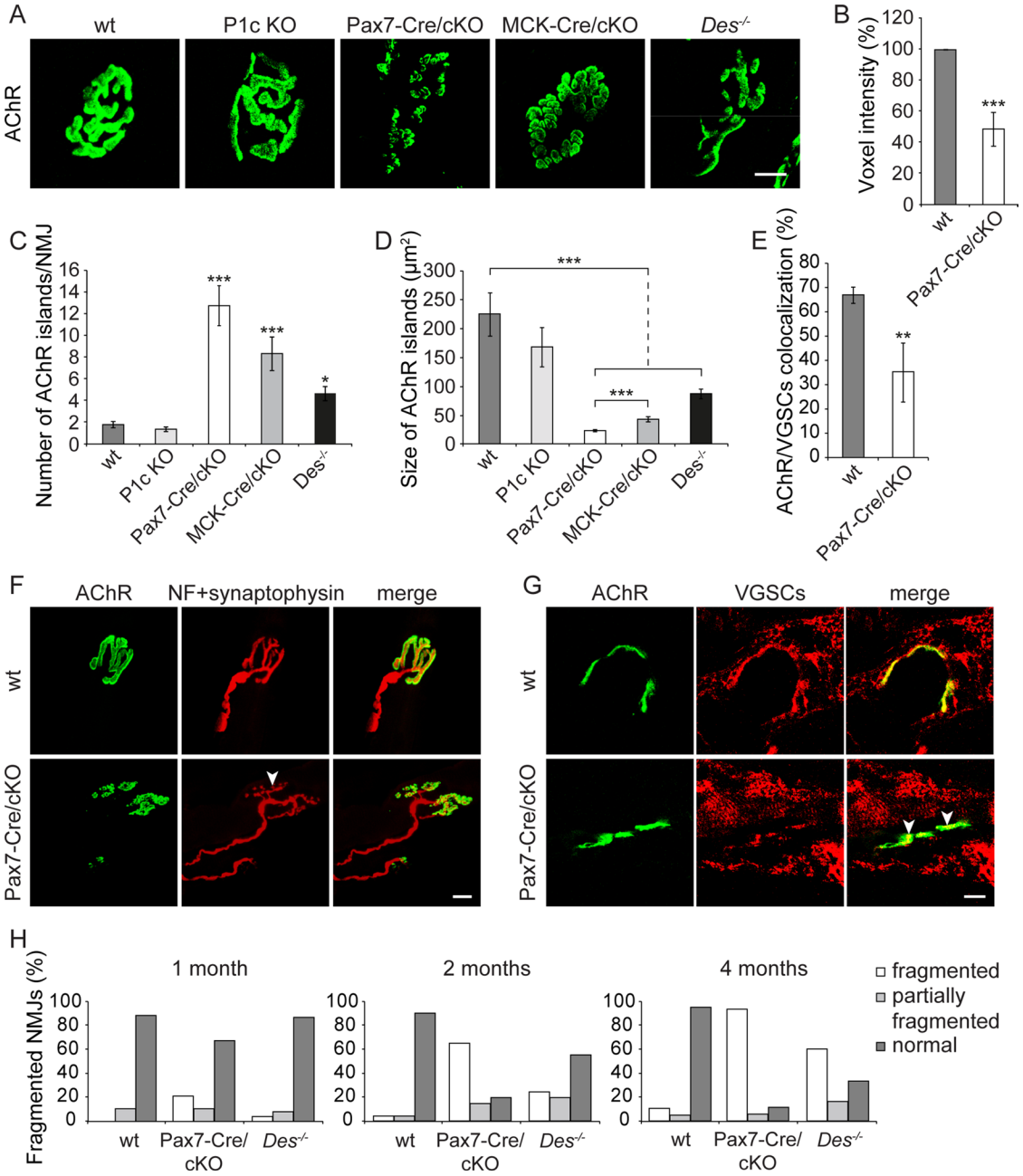

FIGURE 7: Comparative morphometric analyses of NMJs in wt and various mutant mouse lines. (A) Confocal *Z*-stack image projections of Alexa 488–α-BTX–labeled AChR clusters on teased myofibers of soleus muscles. Note fragmented and dispersed NMJ structures in both cKO (Pax7- and MCK-Cre) and *Des*$^{-/-}$ but not in wt and P1c KO mice. (B) Densitometric analysis (voxel intensities) showing ~50% decrement in intensity of Pax7-Cre/cKO in comparison to wt samples (wt, $n = 283$; Pax7-Cre/cKO, $n = 803$). (C, D) Number (C) and size (D) of discrete AChR-positive islands per soleus myofiber NMJs of 2-mo-old mice. NMJs analyzed: wt, 103; P1c KO, 36; MCK-Cre/cKO, 40; Pax7-Cre/cKO, 32; and *Des*$^{-/-}$, 45. (E) Quantification of VGSC-AChR colocalization in wt and Pax7-Cre/cKO muscle. Mean ± SEM (B–D), three experiments. Mean ± SD (E), two experiments. *$p < 0.05$, **$p < 0.01$, and ***$p < 0.001$ compared with wt; unpaired Student's *t* test. (F, G) Teased myofibers (F) or longitudinal sections of soleus muscle (G) derived from wt and Pax7-Cre/cKO mice were double labeled as indicated. Arrowheads, pronounced nerve branching (F) and partial delocalization of VGSCs from receptors (G). Bars, 10 µm (A, F, G). (H) Time course of NMJ fragmentation frequency in plectin- and desmin-deficient soleus muscles. NMJs in soleus muscle fibers of 1-, 2-, and 4-mo-old mice were classified as fragmented (≥6 discontinuous fragments of AChR), partially fragmented (4–5 fragments), and normal (1–3 fragments). Note the early appearance of NMJ fragmentation in Pax7-Cre/cKO mice (1-mo-old) and more dramatic progression with age compared with *Des*$^{-/-}$ mice. A minimum of 30 NMJs were analyzed from each genotype per age.

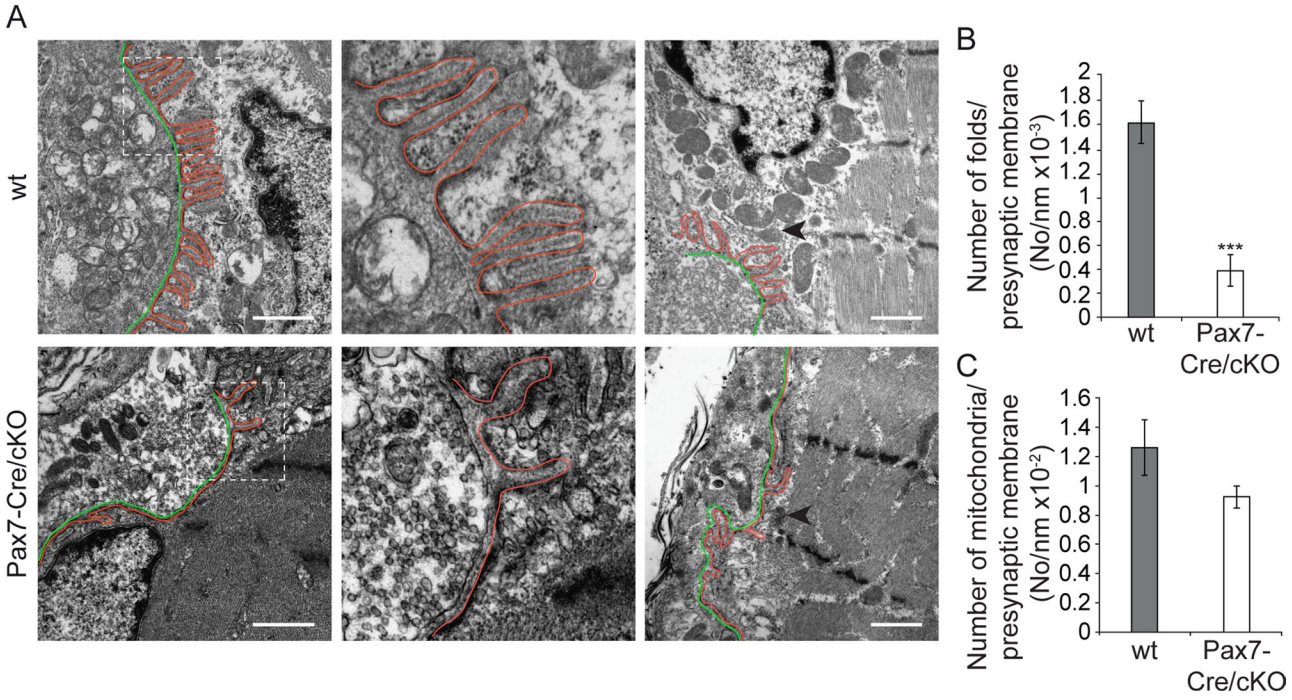

FIGURE 8: Electron microscopy of NMJs in wt and plectin-deficient soleus muscle. (A) Cross-sectioned NMJs show numerous densely assembled synaptic folds of comparable length and upright orientation in wt myofibers, contrasting the mere two or three (mostly curved and disoriented) infoldings formed per presynaptic membrane in mutant mice (left and middle, top vs. bottom row). Middle, 3× magnification of boxed areas in left. Right, survey views showing lower frequency of postsynaptic mitochondria in plectin-deficient compared with wt muscle. Outlining (red), synaptic folds; green, presynaptic membranes. Arrowheads, selected mitochondria. Note disoriented Z-disks in lower right. Bars, 1 µm. (B, C) Numerical evaluation of infoldings (B) and NMJ-associated mitochondria (C), normalized to presynaptic membrane length. Wt, $n = 34$; Pax7-Cre/cKO, $n = 36$. Mean ± SEM, two experiments. ***$p < 0.001$, unpaired Student's *t*-test.

Postsynaptic plectin deficiency leads to impairment of locomotor activity, muscle strength, and limb coordination

To examine whether plectin deficiency affected neuromuscular function, we measured the limb grip strength of adult Pax7-Cre/cKO and wt mice using a grip strength meter. For wt mice, the average maximum grip strength (normalized to body weight) of forelimbs (FLs) and of FLs and hindlimbs (HLs) combined was 5.0 and 8.3 g/g, respectively, whereas the corresponding values for the mutant mice were only 2.5 and 4.3 g/g (Table 1). Alternatively, when limb muscle strength was assessed as the latency of the mouse to let off from an inverted mesh grid (clinging time), in a test series starting at 4 wk of age and running over 10 wk, mutant mice showed a remarkably low latency of ≤10 s, whereas the clinging time of wt mice surpassed the 60-s duration period of the tests (Supplemental Figure S6A). Furthermore, consistent with their pronounced muscle weakness, Pax7-Cre/cKO mice displayed deficits in general locomotor activity and rearing events as analyzed by the open-field test (Table 1 and Supplemental Figure S6B). Assessing whether the motor coordination of adult mice was affected, in the Rotarod test, Pax7-Cre/cKO mice showed a shorter latency in falling off an accelerating rod than their wt littermates (Table 1).

To evaluate more quantitatively the severe deficits in muscle strength and coordination of mutant mice, we measured a variety of locomotor parameters related to the gait of mice during four types of movements—overground walking and wading, skilled walking on a horizontal ladder, and swimming. Tail and intralimb coordination were analyzed by monitoring previously marked bony landmarks and tail regions, such as iliac crest (IC), hip, knee, toe, and the base, middle, and tip of the tail using the MotoRater experimental setup (Supplemental Figure S6, C and D; Zörner *et al.*, 2010). The data obtained in these studies are shown in Tables 2–4. Summarized, these studies confirmed the markedly reduced HL strength of Pax7-Cre/cKO mice and clearly revealed a reduced body–HL coordination, complete loss in body–tail, as well as intratail coordination (Supplemental Videos S9 and S10), and mildly compromised accuracy during skilled walking on a horizontal ladder. Overall these abnormalities resulted in reduced velocity of locomotion, as clearly evident in the wading and swimming tests. In contrast to muscle-restricted plectin deficiency (Pax7-Cre/cKO), presynaptic lack of plectin did not cause reduced muscle strength, as mice deficient in P1c (Fuchs *et al.*, 2009) did not show any signs of muscle weakness, performing indistinguishably from their wt littermates during the inverted mesh grip test (Supplemental Figure S6A). In all, because Pax7-Cre/cKO mice mirrored the pathological features of plectinopathy-associated MyS, such as grossly distorted NMJ morphology, significantly shortened life span, and reduced motility starting from young age (Engel, 2012), they may serve as a useful animal model for the disease.

DISCUSSION

Our study indicates that in fully developed myofibers, AChR–rapsyn complexes, positioned at the crests of postsynaptic infoldings, are physically linked via plectin to the desmin IF network. The isoform of plectin that forms this linkage, P1f, binds in an isoform-dependent manner directly to rapsyn. We demonstrate that this linkage keeps the receptors immobilized in the form of stable clusters and provides mechanical support to the synaptic environment, including the invaginating fold structure.

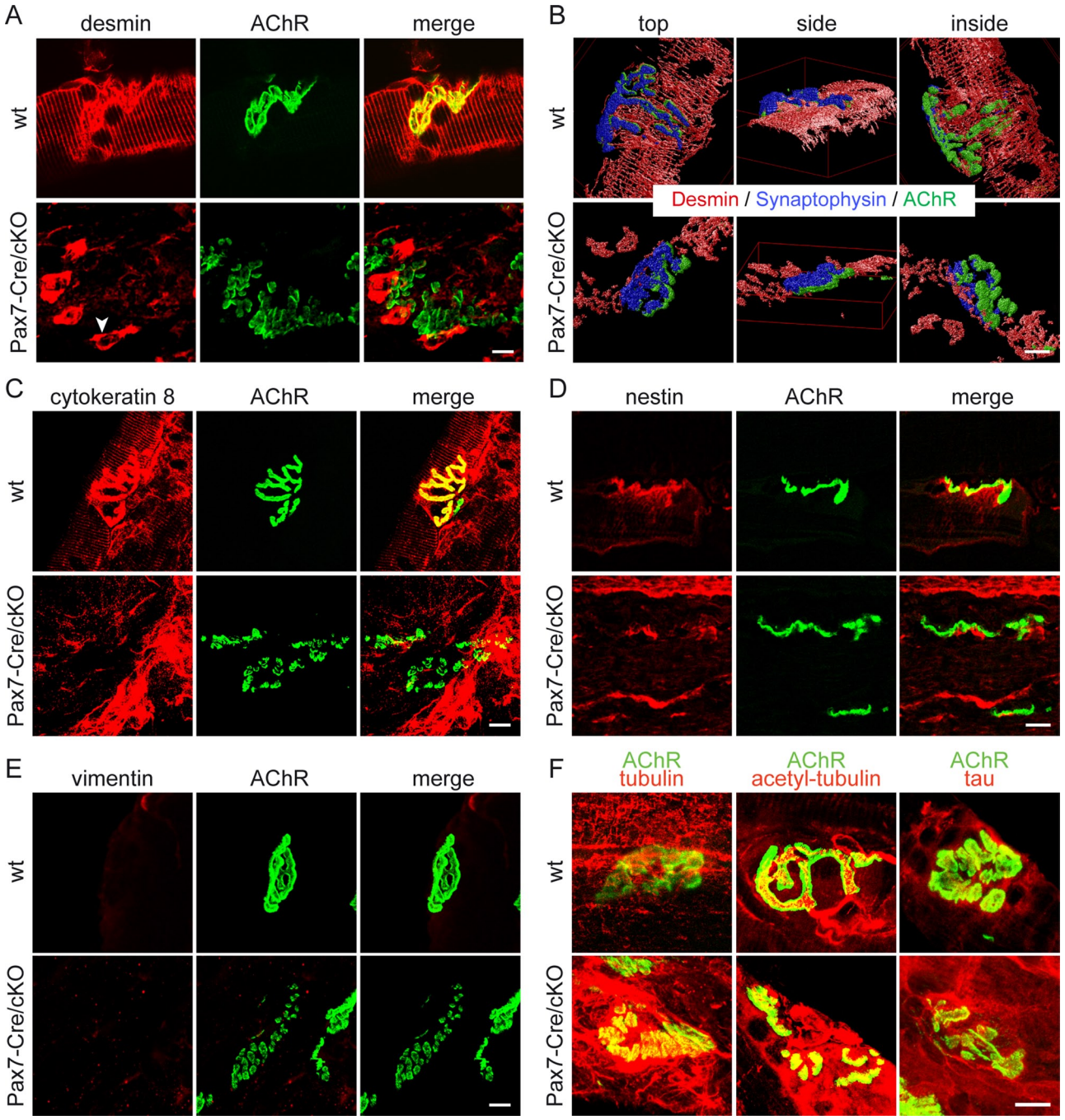

FIGURE 9: Postsynaptic plectin deficiency leads to retraction from NMJs and collapse of IF networks. (A–E) Teased soleus muscle fibers of adult Pax7-Cre/cKO mice and wt littermates labeled with Alexa 488–α-BTX (AChR) and counterstained for the IF proteins desmin (A), cytokeratin 8 (C), nestin (D), or vimentin (E). Note IF-disconnected NMJs in Pax7-Cre/cKO specimens, contrasting the condensed IF lattices surrounding AChRs in wt fibers. Arrowhead in A, pathological aggregates of desmin IFs collapsed around synaptic nuclei. Confocal *Z*-stack images of fibers (triple labeled for desmin, synaptophysin, and AChR) shown in B were reconstructed in three dimensions using Huygens software. (F) Like A, except that muscle fibers were counterstained for tubulin, acetylated tubulin, or the tau protein. Note the more prominent MT networks surrounding endplates, as well as enhanced tau signals in plectin-deficient specimens. Bars, 10 μm.

P1f-specifc sequences prime plectin's ABD for rapsyn binding

The observation that P1f, but not the Z-disk–associated isoform P1d, binds to rapsyn provides a mechanistic explanation for P1f's targeting to NMJs. Our data suggest that the exon 1f–encoded sequence, in contrast to other isoform-specific sequences, promotes rapsyn binding of plectin's ABD. This idea is strongly supported by the high sequence homology of the first exons (as well as of the downstream ABD-encoding regions) of P1f and ACF7/MACF, another cytolinker protein with an ABD that has been implicated in rapsyn binding (Antolik *et al.*, 2007). However, even if both cytolinkers can target rapsyn and mediate actin binding (Andrä *et al.*, 1998; Karakesisoglou *et al.*, 2000), due to its uniqueness as a general IF-binding protein, P1f clearly must exert postsynaptic functions

Test	Parameter	wt	Pax7-Cre/cKO
Grip strength[a]	FLs (g/g)	5.0 ± 0.2	2.6 ± 0.1***
	Total (g/g)	8.3 ± 0.5	4.3 ± 0.2***
Open field[b]	Global distance (m)	77.7 ± 4.2	50.1 ± 28.5***
	Rearing time (min)	12.4 ± 1.5	6.9 ± 0.4***
	Time spent in peripheral sector (%)	66.8 ± 2.7	67.7 ± 3.6
	Time spent in central sector (%)	33.8 ± 2.0	33.5 ± 2.3
Rotarod[c]	Latency of falling (s, day 1)	35.0 ± 2.0	19.1 ± 3.4*
	Latency of falling (s, day 2)	69.7 ± 14.1	40.3 ± 3.5*
	Latency of falling (s, day 3)	92.6 ± 8.3	64.2 ± 1.7

[a]Grip strength of FLs and of FLs and HLs combined (total) of mutant compared with wt mice assessed using a grip strength meter; measurements were normalized to body weight; mice analyzed: wt, 15; Pax7-Cre/cKO, 8. Mean ± SEM.
[b]General locomotor activity (during 30 min) was assessed in open field test; mice analyzed: wt, 28; Pax7-Cre/cKO, 26. Mean ± SEM.
[c]To analyze body balance, the time mice abided on a rotating rod was measured; mice analyzed: wt,12; Pax7-Cre/cKO, 11. Mean ± SEM.
*$p < 0.05$, ***$p < 0.001$, unpaired Student's t-test.

TABLE 1: Muscle strength, locomotor activity, and limb coordination of adult Pax7-Cre/cKO mice.

Parameter	wt	Pax7-Cre/cKO
Identical rungs targeted by FPs and HPs (%)[a]	95.6 ± 0.2	89.5 ± 2.1
Functional paw placement (%)[b]	97.0 ± 0.1	96.2 ± 0.2
Distance between HPs (cm/g)[c]	1.3 ± 0.1	1.9 ± 0.1***

Mice were recorded while walking on a horizontal ladder (see Supplemental Figure S6D). The wt mice crossed the ladder without slipping and by placing the HP on the same rung that previously had been occupied by their ipsilateral forepaw (FP), whereas mutant mice showed a slightly less effective targeting of identical rungs accompanied by several paw slips. Measurements done for each step were averaged. Mice examined: wt, 27; Pax7-Cre/cKO, 20. Mean ± SEM.
[a]FL-HL coordination was assessed by calculating the percentage of identical rungs targeted by ipsilateral FPs and HPs.
[b]Precise placements of FPs on rungs were analyzed, and percentage of paw misplacements was calculated.
[c]The larger distance between HPs suggested loss of HL strength.
***$P < 0.001$, unpaired Student's t test.

TABLE 3: Analysis of skilled locomotion.

that are distinct from those of ACF7/MACF. The observation that agrin was inducing P1f–rapsyn interaction (Figure 5B) speaks for the specificity of the interaction. However, it remains to be shown whether agrin triggers any modification (such as phosphorylation) of rapsyn and/or P1f or of other myoblast proteins that may favor their interaction. Alternatively, P1f could be targeted first to peripheral proteins such as β-dystroglycan (Rezniczek *et al.*, 2007), and only agrin-induced assembly of AChR clusters may bring rapsyn close enough to P1f for interaction to occur. In any case, the severe muscle weakness presented by limb-girdle muscular dystrophy patients due to mutation in P1f's first exon (Gundesli *et al.*, 2010) strongly

	Overground walking		Wading	
Parameter	wt	Pax7-Cre/cKO	wt	Pax7-Cre/cKO
IC (height; mm)	23.6 ± 0.6	19.9 ± 1.2**	25.7 ± 0.9	24.7 ± 0.02
Ankle (height; mm)	14.2 ± 0.3	10.9 ± 0.4	22.3 ± 0.01	17.2 ± 0.2***
Toe (height; mm)	8.4 ± 0.9	5.9 ± 1.5***	11.4 ± 0.5	8.8 ± 0.02*
Base tail (height; mm)	18.5 ± 0.6	14.2 ± 0.9**	20.8 ± 0.04	17.4 ± 0.6
Middle tail (height; mm)	23.9 ± 1.2	7.6 ± 1.3***	19.4 ± 0.4	10.0 ± 0.7*
Tip of the tail (height; mm)[a]	23.6 ± 1.8	2.6 ± 1.3***	11.4 ± 0.1	2.5 ± 0.6*
External rotation of HLs (deg)[b]	25.1 ± 0.9	32.7 ± 2.2***	N.A.	N.A.
Distance between HPs (mm/g)[c]	1.6 ± 0.2	2.3 ± 0.1***	1.7 ± 0.1	2.6 ± 0.1***
Retraction of HLs (deg)[d]	N.A.	N.A.	70.9 ± 1.3	56.3 ± 1.9*
MTP velocity (cm/s)[e]	22.2 ± 1.0	16.0 ± 0.3**	16.3 ± 1.3	9.6 ± 0.7***
Velocity (cm/s)[f]	N.A.	N.A.	19.0 ± 1.6	12.9 ± 0.4**

Mice placed in a long, horizontal compartment were video recorded while walking on dry ground or wading through shallow water (see Supplemental Figure S6D). Each step while walking/wading over the distance of the platform was analyzed, and values were averaged. Note that under both experimental conditions, the heights of different bony landmarks were lower in Pax7-Cre/cKO than in wt control mice, demonstrating weaker body support. Mice examined: wt, 27; Pax7-Cre/cKO, 20. Mean ± SEM. N.A., not analyzed.
[a]Tail dragging suggested abnormal tail coordination.
[b]More extensive external rotation of HLs was measured as the angle between the HL and the anterior–posterior body axis.
[c]The larger distance between hindpaws (HPs) suggested loss of HL strength.
[d]HL retraction (angle between HP-IC and IC-ground axes; see also Supplemental Figure S6D, red lines) during swing phase of HLs appeared more acute in Pax7-Cre/cKO mice, suggesting abnormal iliac crest–HL coordination.
[e]Velocity of metatarsophalangeal joint (MTP) movement.
[f]Note that the speed of wading was significantly lower in Pax7-Cre/cKO than in wt mice.
*$p < 0.05$, **$p < 0.01$, ***$p < 0.001$, unpaired Student's t test.

TABLE 2: Gait analysis during overground walking and wading.

Parameter	wt	Pax7-Cre/cKO
FL strokes[a]	13.5 ± 0.5	33.7 ± 0.7**
Tail's sinusoidal oscillations[b]	18.1 ± 1.3	2.3 ± 0.1***
"Out-of phase" cycles in HLs[c]	0.4 ± 0.1	1.8 ± 0.6
Velocity (cm/s)	36.3 ± 2.5	23.4 ± 1.0***

Mice were video recorded while swimming (see Supplemental Figure S6D and Supplemental Videos S9 and S10). Measurements were made for each stroke and values averaged. Note that in contrast to wt mice, for which the navigation and main driving force during swimming were well-coordinated HL strokes, continuous sinusoidal tail oscillations, and only sporadic FL strokes (see also Supplemental Video S9), Pax7-Cre/cKO mice completely lacked tail oscillations and extensively used their FLs; the latter most probably was a compensatory mechanism for impaired HL function (see also Supplemental Video S10). In addition, in mutant mice, slightly impaired left–right HL coordination during swimming was observed (see also Supplemental Video S10). As a consequence, swimming velocity of Pax7-Cre/cKO mice was reduced ~1.5-fold compared with wt mice. Mice examined: wt, 27; Pax7-Cre/cKO, 20. Mean ± SEM.
[a]Number of FL strokes per distance swum.
[b]Number of tail oscillations upon HL extension.
[c]An "out-of-phase" cycle is when strokes of an identical limb occur in a row. Number of "out-of-phase" cycles per run is shown.
*$p < 0.05$, **$p < 0.01$, ***$p < 0.001$, unpaired Student's *t* test.

TABLE 4: Analysis of swimming locomotion.

attests to the biological significance of the exon 1f–encoded isoform-specific sequence.

Apart from rapsyn, several other postsynaptic proteins residing at the NMJ have been identified as specific binding partners of plectin, including spectrin (Herrmann and Wiche, 1987), ankyrin (Maiweilidan *et al.*, 2011) and the dystrophin–glycoprotein complex (DGC) proteins α-dystrobrevin, utrophin/dystrophin, and β-dystroglycan (Rezniczek *et al.*, 2007; Hijikata *et al.*, 2008). Plectin's interaction sites for some of these proteins have been mapped to molecular domains distant from its N-terminus, making it unlikely that the interactions of P1f with these proteins are isoform dependent. By binding to these proteins via domains other than its N-terminal rapsyn-targeting domain, P1f is likely to strengthen its affinity to the junctional complex and its surroundings, thereby consolidating the compactness of the complex and its immobilization in the IF network. In addition, by connecting IFs to several of the subsarcolemmal membrane proteins along the sides of the folds independently of rapsyn, P1f is likely to contribute to the stabilization of the infolding structure (see later discussion).

NMJ integrity requires the anchorage of AChR clusters into IF networks

Our study shows that the loss of plectin-mediated IF anchorage of AChRs in plectin-deficient muscle leads to a remarkable distortion of endplate architecture, manifesting as fragmentation of the AChR clusters, disturbed topology of nerve terminals, depletion of mitochondria, dramatic degeneration of synaptic folds, and reduced density of clustered receptors and ion channels. At the same time, IF networks retract from peripheral areas and form aggregates, often in juxtanuclear areas. However, the association of AChRs with actin (Figure 2A) and the DGC (implying linkage to the actin cytoskeleton; unpublished data) was maintained, suggesting that IFs rather than cortical actin were responsible for maintaining dense AChR clusters, as well as a normal NMJ morphology and a proper microenvironment. Our analyses and those of others (Agbulut *et al.*, 2001) showed that fragmentation and disorganization of NMJs are observed also in desmin-deficient mice, albeit in general the phenotypic manifestations were less severe. One reason for this difference probably is that plectin deficiency leads to the retraction of all, major (desmin) and minor (keratin, nestin), IF network systems from the endplate domain, whereas in *Des*$^{-/-}$ mice, only the desmin network is affected, enabling compensatory actions of the other systems. However, it remains to be shown whether IFs other than of the desmin type, such as cytokeratins (shown here for the first time to be associated with NMJs), or nestin (previously shown to negatively regulate AChR clustering during embryonic development) (Yang *et al.*, 2011) fulfill synaptic functions that are similar to those of desmin in adult muscle.

As depicted by the model shown in Figure 10A, we suggest that IFs in partnership with plectin serve NMJs in a dual way. First, they promote and consolidate postsynaptic membrane infolding by being linked to AChR/rapsyn complexes at the crest of the folds and to lateral DGCs along the sides of the folds. Second, by physically connecting the endplate region with myonuclei, mitochondria, and Z-disks (via isoforms P1, P1b, and P1d), IFs provide the stable, and at the same time flexible, subsarcolemmal microenvironment around the folds that guarantees efficient force transmission and mechanosensitivity. In contrast, when IFs retract from the endplates and collapse into aggregates in the absence of plectin, endplates lose their typically folded architecture, mobile AChRs remain loose without forming immobilized clusters, and MTs become more prominent (invading the space normally occupied by IFs; Figure 10B).

The reduced clustering of AChRs observed in myotubes deficient in plectin or desmin and the increased mobility of microclusters in plectin-deficient myotubes due to desmin collapse most probably were the effects of lost IF anchorage combined with preferential linkage to the cortical actin network, which has been shown to be responsible for AChR redistribution (Dai *et al.*, 2000). In agreement with this conception is the reduction of microcluster mobility after treatment of plectin-deficient myotubes with cytochalasin D (unpublished data), as well as the live imaging of microcluster movement along actin fibers (unpublished data). Furthermore, the highly enriched subsynaptic MT network found in plectin-deficient muscle as a consequence of IF collapse may be responsible for excessive delivery not only of membrane proteins (e.g. GLUT4; Raith *et al.*, 2013) toward the endplate region, but also of regulators and executers of the agrin signaling pathway. Given that tau protein binds with high affinity to Src protein kinases (Lee *et al.*, 1998), the observed accumulation of tau-studded MTs at endplates of plectin-deficient myocytes in place of IF networks could easily contribute to the massing up of tyrosine protein kinases in the NMJ domain, leading to the unbalanced agrin signaling and compromised AChR clustering.

In conclusion, our study uncovered a crucial role of plectin in stabilizing AChR clusters at NMJs. We found that P1f in an isoform-dependent manner binds directly to rapsyn and reverses the pathology of abnormal cluster formation by immobilizing the AChR complex on the desmin IF network. Without such linkage, the IF network collapses and forms aggregates, NMJs lose their characteristic infolding pattern, and AChRs become mobile and clustering incompetent. This study also adds another important facet to the global role of plectin isoforms as organizers and functional determinants of IF networks. The essentiality of P1f's functional partnership with desmin IFs for NMJs integrity matches that of P1a and keratin IFs for hemidesmosomes in basal keratinocytes and of P1f, respectively P1, and vimentin IFs for adhesion complexes in fibroblasts and Schwann cells (Andrä *et al.*, 2003; Burgstaller *et al.*, 2010; Walko *et al.*, 2013). Extending the role of cytolinkers and IFs to synapses, this study provides a fertile ground to investigate analogous plectin-mediated functions in the CNS, especially as P1c, the major isoform of plectin

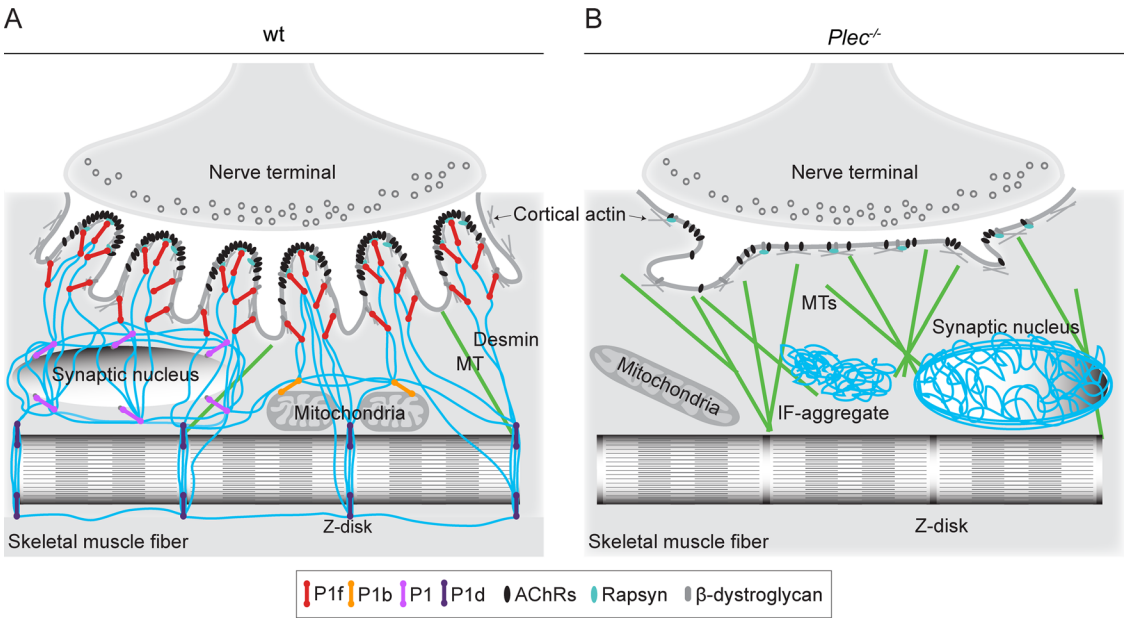

FIGURE 10: Schematic model of endplate regions depicting cytoskeleton anchorage in wt and plectin-deficient myofibers. (A) In normal myofibers, plectin isoform P1f, specifically bound via its N-terminal molecular domain to endplates, recruits desmin IFs (in blue) via its C-terminal IFBD; in addition, P1f interlinks IFs with DGC constituent proteins laterally along the infoldings. In a similar way, other isoforms of plectin specifically link the nuclear/ER membrane (P1), mitochondria (P1b), and Z-disks (P1d) to the IF network. In this way, a highly organized IF network mechanically integrates endplates, cytoplasmic organelles, and the contractile apparatus, stabilizing the synaptic microenvironment and enabling incorporation of AChRs into stable clusters. (B) In plectin-deficient myofibers, the IF network becomes unbound from endplates and the sarcolemma, leading to its collapse and aggregation. This causes marked architectural abnormalities of endplates (such as loss of infoldings), reduced AChR cluster stability, and profound changes in the synaptic microenvironment, including altered morphology of myonuclei (unpublished data) and mitochondria, as well as accumulation of MTs (in green).

expressed in neural cells, is enriched in postsynaptic dendrites (Fuchs *et al.*, 2009). On a final note, the Pax7-Cre/cKO mouse line could become a useful tool for developing treatment strategies for plectinopathies and other myopathies, including desminopathies, manifesting with myasthenic syndrome.

MATERIALS AND METHODS

Mice

Animal studies were approved by the Federal Ministry for Science, Research and Economy, Vienna, Austria. Pax7-Cre/cKO mice were generated by crossing Pax7-Cre mice (Keller *et al.*, 2004) to plectin$^{flox/flox}$ mice (Ackerl *et al.*, 2007) until reaching homozygosity for both transgenes (Pax7-Cre/cKO). Control mice referred to as wt were homozygous for the Cre transgene and either homozygous or heterozygous for the floxed plectin gene. Desmin-knockout (provided by D. Paulin, Université Paris, Paris, France), MCK-Cre/cKO, and P1c KO mice have been described (Li *et al.*, 1996; Konieczny *et al.*, 2008; Fuchs *et al.*, 2009). Because no differences in phenotypes were observed between genders, data obtained from male and female mice having the same genotype were pooled in all experiments.

Antibodies

The following primary antibodies (Abs) were used for immunofluorescence microscopy (IFM), immunoblotting (IB), and immunoprecipitation (IP): rabbit antisera (As) to plectin (#46, IFM) (Andrä *et al.*, 2003) and synaptophysin (IFM; Life Technologies, Carlsbad, CA); guinea pig As to cytokeratin 8 (IFM; Denk *et al.*, 1982); affinity-purified (a.p.) rabbit Abs to P1f (IFM, IB; Rezniczek *et al.*, 2007), P1 (IFM; Abrahamsberg *et al.*, 2005) and a.p. goat Abs to vimentin (IFM; Giese and Traub, 1986); mouse monoclonal (m) Abs to AChRα subunit (IB; BD Bioscience, San Jose, CA), rapsyn (IP, IB; Thermo Scientific, Waltham, MA), GST-tag (IP, IB; Sigma-Aldrich, St. Louis, MO), His-tag (IP, IB; Qiagen, Venlo, Limburg, Netherlands), HA-tag (IB; Covance, Princeton, NJ), HA-tag (IP; Sigma-Aldrich), α-tubulin (IFM; clone T5168; Sigma-Aldrich), acetylated tubulin (IFM; clone T6793; Sigma-Aldrich), desmin (IFM, IB; clone D33; Dako, Glostrup, Denmark), pax7 (Developmental Studies Hybridoma Bank, Iowa City, IA), and VGSCs (IFM; provided by R. Barchi, University of Pennsylvania, Philadelphia, PA; Casadei *et al.*, 1984); rabbit mAbs to nestin (IFM; Covance); rabbit Abs to tau (IFM, IB; clone A0028; Dako), and neurofilament heavy chain (IFM; clone RT97, Developmental Studies Hybridoma Bank). As secondary Abs, we used donkey Rhodamine Red anti-mouse, -rat, and -guinea pig, goat Rhodamine Red anti-rabbit, donkey Alexa 647 anti-mouse and anti-rabbit, and donkey Texas Red anti-goat immunoglobulin Gs (IgGs) for IFM (all from Jackson ImmunoResearch, West Grove, PA), and goat horseradish peroxidase–conjugated anti-mouse and -rat (Jackson ImmunoResearch) and anti-rabbit (Vector Laboratories, Burlingame, CA) IgGs for IB. Alexa 488– or biotin-conjugated BTX (Molecular Probes, Eugene, OR), Cy5-streptavidin, and Rhodamine Red–streptavidin (Jackson ImmunoResearch) were used for visualization or pull down of AChRs.

cDNA constructs

cDNA constructs encoding truncated (N-terminal) or full-length versions of isoforms P1f, P1, and P1d (fused to C-terminal enhanced GFP) have been described (Rezniczek *et al.*, 2003). For bacterial

expression of plectin fragments, cDNAs encoding exons P1f-8, P1d-8, and 2-8 (Rezniczek *et al.*, 2003) were subcloned into modified pET-15b vector (Novagen, Darmstadt, Germany). Variant P1f-rodless (pGR367) corresponds to full-length plectin without exon 30 (Elliott *et al.*, 1997), subcloned into pEGFP-N2 (BD Clontech, Palo Alto, CA). pKG31 (P1f-Ins16) was generated by exchanging the mouse plectin cDNA sequence encoding P1f's C-terminal 83 amino acids with a fragment of human cDNA that includes the 16–base pair insertion mutation (13803ins) and the new 47–amino acid residue–long tail arising due to the frameshift (Schröder *et al.*, 2002) and subcloning the hybrid construct into pEGFP-C1 (BD Clontech). For agrin expression, plasmid C-Ag 4.8 encoding neural agrin was used (Ferns *et al.*, 1993). cDNA encoding mouse rapsyn fused to a C-terminal HA tag was subcloned into pcDNA3.1 (Life Technologies). Expression plasmids for GFP-tagged AChRε-subunit (me-GFP-pRK5) (Gensler *et al.*, 2001), desmin-GFP (Winter *et al.*, 2014), and rapsyn-GST (Zhang *et al.*, 2007) were kindly provided by V. Witzemann (Max Planck Institute, Heidelberg, Germany), M. C. Walter (Ludwig-Maximilians-Universität, Munich, Germany), and L. Mei (Georgia Regents University, Augusta, GA), respectively.

Immunohistochemistry and electron microscopy of muscle tissue

Preparation and immunostaining of teased fibers of limb muscles and muscle sections were as described (Konieczny *et al.*, 2008). Processing of soleus muscle for electron microscopy was carried out as described Konieczny *et al.* (2008), except for additional acetylcholinesterase staining (Karnovsky and Roots, 1964) after muscle dissection. Morphometric ultrastructural analyses were performed using analySIS FIVE software (Soft Imaging System, Muenster, Germany).

Myocyte cultivation, manipulation, and AChR clustering

Primary myoblasts were isolated from neonatal skeletal limb muscles of mice, spread onto collagen-coated culture dishes, and cultivated in 20% fetal calf serum (FCS) and basic fibroblast growth factor–supplemented growth medium (for details see Winter *et al.*, 2014). Immortalized (*Plec*$^{+/+}$ and *Plec*$^{-/-}$) myoblasts (Winter *et al.*, 2014) were cultivated under similar, and C2C12 cells under standard (DMEM, 10% FCS), conditions. To induce differentiation, myoblasts of all types were switched to DMEM containing 5% horse serum (fusion medium). Transient transfection of myoblasts with cDNA expression plasmids was achieved by nucleofection, using Amaxa Nucleofector kit for human dermal fibroblasts (VAPD-1001; Lonza, Basel, Switzerland). To induce IF collapse or MT stabilization, differentiated myotubes were treated (16 h) with agrin-conditioned medium (see later description) and subsequently incubated with 0.1 µg/ml OA (Calbiochem, San Diego, CA), 1 µM WFA (ChromaDex, Irvine, CA), or 0.5 µM Taxol (Sigma-Aldrich) for 3 h at 37°C.

To induce AChR clustering, myotubes were incubated in agrin-conditioned medium for up to 16 h. Clusters were visualized by incubation with 0.2 µg/ml Alexa 488–α-BTX for 45 min at 37°C, rinsing in phosphate-buffered saline (PBS), fixation with 2% paraformaldehyde, and mounting in Mowiol. When myoblasts were transfected with expression plasmids encoding GFP-tagged proteins, AChR clusters were treated with 0.2 µg/ml biotin-BTX for 45 min at 37°C, followed by incubation with Rhodamine Red–conjugated streptavidin for 30 min at 37°C. For immunostaining after AChR labeling, myotubes were fixed, washed, and immunolabeled as described previously (Winter *et al.*, 2008). To analyze the stability of agrin-induced clusters, myotubes (exposed to agrin overnight) were washed and kept in agrin-free fusion medium for 4–10 h, followed by AChR labeling.

Agrin-conditioned medium was prepared by transient transfection of HEK 293T cells with cDNA expression plasmids for neural agrin. AChR-clustering activity of agrin-conditioned medium was assessed using differentiated C2C12 myotubes according to Herbst and Burden (2000).

Confocal microscopy, image processing, and morphometric analyses

Images of tissue sections and teased muscle fibers were recorded with a fluorescence laser scanning microscope (LSM710; Carl Zeiss, Jena, Germany) equipped with a Plan-Apochromat 63×/1.4 numerical aperture (NA) objective lens and Zeiss ZEN (2010) software. For visualization of AChR clusters on cultured myotubes, ~20 random nonoverlapping fields/dish ($n \geq 3$ dishes) were imaged using an LSM510 microscope (Carl Zeiss) equipped with a Plan-Apochromat 40×/1.3 NA objective lens. All images were processed using ImageJ (version 1.43; National Institutes of Health, Bethesda, MD) and Photoshop CS4 (Adobe, San Jose, CA) software packages. To measure cluster densities in cultured myotubes, confocal images were recorded below fluorescence intensity saturation levels, and fluorescence emission intensities of distinct clusters were measured using ImageJ. For endplate morphometry, maximum intensity projections of NMJs were made using ImageJ, and the number and area of discrete Alexa 488–positive islands per NMJ were quantified. Deconvolution of *Z*-stack images was done with Huygens Professional software (version 4.4; SVI, Hilversum, Netherlands) using blind deconvolution. Three-dimensional reconstruction of desmin filament networks at NMJs was done after deconvolution of immunostained tissue fibers and surface rendering using the Surface Renderer tool (Huygens Professional). To assess AChR densities at endplates, voxel intensities of discrete AChR islands (recorded below fluorescence intensity saturation levels) were measured after deconvolution of Alexa 488–α-BTX–labeled AChRs images using the Object Analyzer tool (Huygens Professional); data were analyzed as in Leu *et al.* (2003). VGSC/AChR colocalization (percentage of overlapping green and red pixels), areas, mean intensities, and total number of AChR clusters were analyzed using ImageJ software. Number of clusters (≥5 or <5 µm^2 was normalized to the total visible area of the myotubes.

Live imaging and tracking of receptors

To monitor AChR cluster stability, differentiated myotubes adhering to EHS laminin (Sigma-Aldrich)–coated dishes (Ibidi, Munich, Germany) were exposed to agrin (16 h), washed twice in fusion medium without agrin, and labeled (in sequence) with biotin–α-BTX and Rhodamine Red–streptavidin (30 min, 37°C each). After labeling, cells were subjected to time-lapse microscopy using a Zeiss LSM710 confocal microscope equipped with a heated stage (37°C) and constant 5% CO_2 flow and a Plan-Apochromat 63×/1.4 NA objective lens. Images were taken at 15-s intervals during 1- to 2-h recordings using the Time Series tool (ZEN 2009). To monitor AChR mobility after inducing IF collapse, 0.1 µg/ml OA or 1 µM WFA was added to the growth medium before recording. Mobility of individual clusters was traced using the Manual Tracking plug-in from the ImageJ software. Alexa 488–α-BTX–labeled AChRs were monitored in a similar way at 2-h intervals during a 10-h period after agrin withdrawal. For monitoring cluster formation in AChRε-GFP–transfected myotubes, GFP-positive signals were recorded after addition of agrin, and frames were taken at 2-s intervals for up to 1 h.

Protein purification, in vitro binding assay, and immunoblotting

Rapsyn-GST, GST, and His-tagged recombinant protein fragments were expressed in *Escherichia coli* BL21 (DE3) and purified as described in Rezniczek *et al.* (2004). For GST pull-down assays, rapsyn-GST, immobilized on glutathione Sepharose (GE Healthcare, Fairfield, CT), was incubated with His-tagged plectin variants, followed by washing and elution. Uncoupled or GST protein–coupled glutathione Sepharose beads were used as negative controls. For immunoblotting analysis, proteins were separated by 6, 10, or 12% SDS–PAGE, transferred to nitrocellulose membranes (blocked with 5% bovine serum albumin in Tris-buffered saline/0.1% Tween 20) before incubations with Abs. Chemiluminescence was detected with Fusion FX7 system (Peqlab, Erlangen, Germany), and bands were quantified with QuantiScan software (Biosoft, Palo Alto, CA).

AChR pull down, extractability, and rapsyn coimmunoprecipitation from cell lysates

The preparation of lysates from cultivated cells has been described in Winter *et al.* (2014). Membrane-bound AChRs were isolated according to Borges and Ferns (2001). To assess association of P1f with AChRs, equal aliquots of eluates were analyzed on 10% (AChRα) and 6% (P1f) gels. For AChR extractability assays, a modified protocol of Sadasivam *et al.* (2005) was followed. Differentiated myotubes (treated or untreated with agrin for 1 h) were washed briefly in ice-cold PBS (supplemented with 1 mM Na orthovanadate) before addition of lysis buffer (30 mM triethanolamine, pH 7.5, 50 mM NaCl, 5 mM EDTA, 5 mM ethylene glycol tetraacetic acid, complete mini protease inhibitor cocktail [Roche, Basel, Switzerland] and phosphatase inhibitor cocktails 1 and 3 [Sigma-Aldrich]) supplemented with Triton X-100 at a final concentration of 0.01%. Extraction was for 15 min. Cells were scraped from each dish, homogenized by pipetting up and down 10 times, and transferred to tubes that were rotated for 5 min. Extracts were centrifuged for 3 min at 13,600 × *g* at 4°C in a table-top centrifuge, and supernatants (first extraction) were collected. Pellets were resuspended in lysis buffer containing 0.03% Triton X-100 and similarly extracted to yield supernatants (second extraction). Pellets were subjected to two further extractions using lysis buffers supplemented with Triton X-100 at final concentrations of 0.1 and 1%, respectively (third and fourth extractions). All extractions were then subjected to AChR pull-down assays using biotinylated α-BTX, followed by immunoblotting for AChRα subunit. For immunoprecipitation (IP) of rapsyn, differentiated C2C12 myoblasts were lysed in 150 mM NaCl, 50 mM Tris-Cl, pH 7.4, 1% NP-40, 1 mM EDTA, 0.25% Na deoxycholate, 1 mM phenylmethylsulfonyl fluoride, and 1 mM Na_3VO_4 supplemented with complete mini protease inhibitor cocktail (Roche) and phosphatase inhibitor cocktails 1 and 3 (Sigma-Aldrich). For IP of rapsyn-HA, HEK 293T cells (transiently coexpressing rapsyn-HA and GFP-tagged plectin variants) were grown to confluence on 78-cm^2 culture dishes; cells were homogenized, and after centrifugation (13,600 × *g*, 5 min, 4°C), supernatants were subjected to IP using HA tag–specific antibodies and protein G–agarose beads (Pierce, Rockford, IL). Lysates of HEK cells (transiently expressing GFP-tagged plectin variants, but no rapsyn-HA) were used as negative controls.

Muscle strength measurements and locomotor analyzes

Using the grip strength meter (Bioseb, Vitrolles, France), we assessed muscular strength as previously described (Winter *et al.*, 2014). To assess the exploratory behavior and general locomotor activity in a new environment, mice were exposed to the open-field test and recorded using a video tracking system (TSE Systems, Bad Homburg, Germany). For coordination and motor balance evaluation, up to five mice were placed on a rod (TSE Systems) rotating with an accelerating mode (4–40 rpm) for 5 min/trial. Four trials with an intertrial interval of 15 min were performed for three consecutive days. To quantify a more refined locomotor function, we subjected the animals to skilled walking (overground and on ladder), wading, and swimming locomotion, using the MotoRater system (TSE Systems) following the protocols as described in Zörner *et al.* (2010).

Statistical evaluation

Comparisons between two groups or values of multiple groups were made using an unpaired, two-tailed Student's *t* test ($\alpha = 0.05$) or one-way analysis of variance (ANOVA; $\alpha = 0.05$), respectively. The significance between values of individual groups and controls was subsequently determined using Tukey's posthoc test.

ACKNOWLEDGMENTS

We thank D. Paulin (Université Paris, Paris, France) for originally providing desmin-knockout mice and E. Wagner (Centro Nacional de Investigaciones Oncológicas, Madrid, Spain) for Pax7-Cre mice, originally obtained from M. Capecchi (University of Utah, Salt Lake City, UT). This work was supported by Grants I413-B09 (part of the Multilocation DFG-Research Unit 1228, Molecular Pathogenesis of Myofibrillar Myopathies) and P23729-B11 and Doctoral Program Grant W1220 from the Austrian Science Fund, the Hochschuljubiläumsstiftung der Stadt Wien (H-2079-2012), and NanoNet COST Action (BM 1002).

REFERENCES

Abrahamsberg C, Fuchs P, Osmanagic-Myers S, Fischer L, Propst F, Elbe-Bürger A, Wiche G (2005). Targeted ablation of plectin isoform 1 uncovers role of cytolinker proteins in leukocyte recruitment. Proc Natl Acad Sci USA 102, 18449–18454.

Ackerl R, Walko G, Fuchs P, Fischer I, Schmuth M, Wiche G (2007). Conditional targeting of plectin in prenatal and adult mouse stratified epithelia causes keratinocyte fragility and lesional epidermal barrier defects. J Cell Sci 120, 2435–2443.

Agbulut O, Li Z, Périé S, Ludosky MA, Paulin D, Cartaud J, Butler-Browne G (2001). Lack of desmin results in abortive muscle regeneration and modifications in synaptic structure. Cell Motil Cytoskeleton 49, 51–66.

Andrä K, Kornacker I, Jörgl A, Zörer M, Spazierer D, Fuchs P, Fischer I, Wiche G (2003). Plectin-isoform-specific rescue of hemidesmosomal defects in plectin (-/-) keratinocytes. J Invest Dermatol 120, 189–197.

Andrä K, Nikolic B, Stöcher M, Drenckhahn D, Wiche G (1998). Not just scaffolding: plectin regulates actin dynamics in cultured cells. Genes Dev 12, 3442–3451.

Antolik C, Catino DH, O'Neill AM, Resneck WG, Ursitti JA, Bloch RJ (2007). The actin binding domain of ACF7 binds directly to the tetratricopeptide repeat domains of rapsyn. Neuroscience 145, 56–65.

Banwell BL, Russel J, Fukudome T, Shen XM, Stilling G, Engel AG (1999). Myopathy, myasthenic syndrome, and epidermolysis bullosa simplex due to plectin deficiency. J Neuropathol Exp Neurol 58, 832–846.

Bargagna-Mohan P, Hamza A, Kim YE, Khuan Abby Ho Y, Mor-Vaknin N, Wendschlag N, Liu J, Evans RM, Markovitz DM, Zhan CG, *et al.* (2007). The tumor inhibitor and antiangiogenic agent withaferin A targets the intermediate filament protein vimentin. Chem Biol 14, 623–634.

Borges LS, Ferns M (2001). Agrin-induced phosphorylation of the acetylcholine receptor regulates cytoskeletal anchoring and clustering. J Cell Biol 153, 1–12.

Burden S (1982). Identification of an intracellular postsynaptic antigen at the frog neuromuscular junction. J Cell Biol 94, 521–530.

Burgstaller G, Gregor M, Winter L, Wiche G (2010). Keeping the vimentin network under control: cell-matrix adhesion-associated plectin 1f affects cell shape and polarity of fibroblasts. Mol Biol Cell 21, 3362–3375.

Carlsson L, Li Z, Paulin D, Thornell LE (1999). Nestin is expressed during development and in myotendinous and neuromuscular junctions in wild type and desmin knock-out mice. Exp Cell Res 251, 213–223.

Casadei JM, Gordon RD, Lampson LA, Schotland DL, Barchi RL (1984). Monoclonal antibodies against the voltage-sensitive Na+ channel from mammalian skeletal muscle. Proc Natl Acad Sci USA 81, 6227–6231.
Castañón MJ, Walko G, Winter L, Wiche G (2013). Plectin-intermediate filament partnership in skin, skeletal muscle, and peripheral nerve. Histochem Cell Biol 140, 33–53.
Dai Z, Luo X, Xie H, Peng HB (2000). The actin-driven movement and formation of acetylcholine receptor clusters. J Cell Biol 150, 1321–1334.
Denk H, Krepler R, Lackinger E, Artlieb U, Franke WW (1982). Immunological and biochemical characterization of the keratin-related component of Mallory bodies: a pathological pattern of hepatocytic cytokeratins. Liver 2, 165–175.
Elliott CE, Becker B, Oehler S, Castañón MJ, Hauptmann R, Wiche G (1997). Plectin transcript diversity: identification and tissue distribution of variants with distinct first coding exons and rodless isoforms. Genomics 42, 115–125.
Engel AG (2012). Current status of the congenital myasthenic syndromes. Neuromuscul Disord 22, 99–111.
Ferns MJ, Campanelli JT, Hoch W, Scheller RH, Hall Z (1993). The ability of agrin to cluster AChRs depends on alternative splicing and on cell surface proteoglycans. Neuron 11, 491–502.
Forrest K, Mellerio JE, Robb S, Dopping-Hepenstal PJ, McGrath JA, Liu L, Buk SJ, Al-Sarraj S, Wraige E, Jungbluth H (2010). Congenital muscular dystrophy, myasthenic symptoms and epidermolysis bullosa simplex (EBS) associated with mutations in the PLEC1 gene encoding plectin. Neuromuscul Disord 20, 709–711.
Fuchs P, Zörer M, Reipert S, Rezniczek GA, Propst F, Walko G, Fischer I, Bauer J, Leschnik MW, Lüscher B, *et al*. (2009). Targeted inactivation of a developmentally regulated neural plectin isoform (plectin 1c) in mice leads to reduced motor nerve conduction velocity. J Biol Chem 284, 26502–26509.
Fuchs P, Zörer M, Rezniczek GA, Spazierer D, Oehler S, Castañón MJ, Hauptmann R, Wiche G (1999). Unusual 5′ transcript complexity of plectin isoforms: novel tissue-specific exons modulate actin binding activity. Hum Mol Genet 8, 2461–2472.
Gensler S, Sander A, Korngreen A, Traina G, Giese G, Witzemann V (2001). Assembly and clustering of acetylcholine receptors containing GFP-tagged epsilon or gamma subunits: selective targeting to the neuromuscular junction in vivo. Eur J Biochem 268, 2209–2217.
Giese G, Traub P (1986). Induction of vimentin synthesis in mouse myeloma cells MPC-11 by 12-0-tetradecanoylphorbol-13-acetate. Eur J Cell Biol 40, 266–274.
Gregor M, Osmanagic-Myers S, Burgstaller G, Wolfram M, Fischer I, Walko G, Resch GP, Jörgl A, Herrmann H, Wiche G (2014). Mechanosensing through focal adhesion-anchored intermediate filaments. FASEB J 28, 715–729.
Gundesli H, Talim B, Korkusuz P, Balci-Hayta B, Cirak S, Akarsu NA, Topaloglu H, Dincer P (2010). Mutation in exon 1f of PLEC, leading to disruption of plectin isoform 1f, causes autosomal-recessive limb-girdle muscular dystrophy. Am J Hum Genet 87, 834–841.
Herbst R, Burden SJ (2000). The juxtamembrane region of MuSK has a critical role in agrin-mediated signaling. EMBO J 19, 67–77.
Herrmann H, Wiche G (1987). Plectin and IFAP-300K are homologous proteins binding to microtubule-associated protein-1 and protein-2 and to the 240 kD subunit of spectrin. J Biol Chem 262, 1320–1325.
Hijikata T, Nakamura A, Isokawa K, Imamura M, Yuasa K, Ishikawa R, Kohama K, Takeda S, Yorifuji H (2008). Plectin 1 links intermediate filaments to costameric sarcolemma through beta-synemin, alpha-dystrobrevin and actin. J Cell Sci 121, 2062–2074.
Janmey PA, Euteneuer U, Traub P, Schliwa M (1991). Viscoelastic properties of vimentin compared with other filamentous biopolymer networks. J Cell Biol 113, 155–160.
Karakesisoglou I, Yang Y, Fuchs E (2000). An epidermal plakin that integrates actin and microtubule networks at cellular junctions. J Cell Biol 149, 195–208.
Karnovsky MJ, Roots L (1964). A "direct-coloring" thiocholine method for cholinesterases. J Histochem Cytochem 12, 219–221.
Keller C, Hansen MS, Coffin CM, Capecchi MR (2004). Pax3 : Fkhr interferes with embryonic Pax3 and Pax7 function: implications for alveolar rhabdomyosarcoma cell of origin. Genes Dev 18, 2608–2613.
Konieczny P, Fuchs P, Reipert S, Kunz WS, Zeöld A, Fischer I, Paulin D, Schröder R, Wiche G (2008). Myofiber integrity depends on desmin network targeting to Z-disks and costameres via distinct plectin isoforms. J Cell Biol 181, 667–681.
Kreplak L, Herrmann H, Aebi U (2008). Tensile properties of single desmin intermediate filaments. Biophys J 94, 2790–2799.
Lee CW, Han J, Bamburg JR, Han L, Lynn R, Zheng JQ (2009). Regulation of acetylcholine receptor clustering by ADF/cofilin-directed vesicular trafficking. Nat Neurosci 12, 848–856.
Lee G, Newman ST, Gard DL, Band H, Panchamoorthy G (1998). Tau interacts with src-family non-receptor tyrosine kinases. J Cell Sci 111, 3167–3177.
Leu M, Bellmunt E, Schwander M, Fariñas I, Brenner HR, Müller U (2003). Erbb2 regulates neuromuscular synapse formation and is essential for muscle spindle development. Development 130, 2291–2301.
Li Z, Colucci-Guyon E, Pinçon-Raymond M, Mericskay M, Pournin S, Paulin D, Babinet C (1996). Cardiovascular lesions and skeletal myopathy in mice lacking desmin. Dev Biol 175, 362–366.
Maiweilidan Y, Klauza I, Kordeli E (2011). Novel interactions of ankyrins-G at the costameres: the muscle-specific Obscurin/Titin-Binding-related Domain (OTBD) binds plectin and filamin C. Exp Cell Res 317, 724–736.
Marchand S, Bignami F, Stetzkowski-Marden F, Cartaud J (2000). The myristoylated protein rapsyn is cotargeted with the nicotinic acetylcholine receptor to the postsynaptic membrane via the exocytic pathway. J Neurosci 20, 521–528.
Maselli R, Arredondo J, Cagney O, Mozaffar T, Skinner S, Yousif S, Davis R, Gregg J, Sivak M, Konia T, *et al*. (2010). Congenital myasthenic syndrome associated with epidermolysis bullosa caused by homozygous mutations in PLEC1 and CHRNE. Clin Genet 80, 444–451.
Mitsui T, Kawajiri M, Kunishige M, Endo T, Akaike M, Aki K, Matsumoto T (2000). Functional association between nicotinic acetylcholine receptor and sarcomeric proteins via actin and desmin filaments. J Cell Biochem 77, 584–595.
Mucke N, Kreplak L, Kirmse R, Wedig T, Herrmann H, Aebi U, Langowski J (2004). Assessing the flexibility of intermediate filaments by atomic force microscopy. J Mol Biol 335, 1241–1250.
Osmanagic-Myers S, Gregor M, Walko G, Burgstaller G, Reipert S, Wiche G (2006). Plectin-controlled keratin cytoarchitecture affects MAP kinases involved in cellular stress response and migration. J Cell Biol 174, 557–568.
Raith M, Valencia RG, Fischer I, Orthofer M, Penninger JM, Spuler S, Rezniczek GA, Wiche G (2013). Linking cytoarchitecture to metabolism: sarcolemma-associated plectin affects glucose uptake by destabilizing microtubule networks in mdx myofibers. Skelet Muscle 3, 14.
Relaix F, Rocancourt D, Mansouri A, Buckingham M (2005). A Pax3/Pax7-dependent population of skeletal muscle progenitor cells. Nature 435, 948–953.
Rezniczek GA, Abrahamsberg C, Fuchs P, Spazierer D, Wiche G (2003). Plectin 5′-transcript diversity: short alternative sequences determine stability of gene products, initiation of translation and subcellular localization of isoforms. Hum Mol Genet 12, 3181–3194.
Rezniczek GA, Janda L, Wiche G (2004). Plectin. Methods Cell Biol 78, 721–755.
Rezniczek GA, Konieczny P, Nikolic B, Reipert S, Schneller D, Abrahamsberg C, Davies KE, Winder SJ, Wiche G (2007). Plectin 1f scaffolding at the sarcolemma of dystrophic (mdx) muscle fibers through multiple interactions with beta-dystroglycan. J Cell Biol 176, 965–977.
Sadasivam G, Willmann R, Lin S, Erb-Vögtli S, Kong XC, Rüegg MA, Fuhrer C (2005). Src-family kinases stabilize the neuromuscular synapse in vivo via protein interactions, phosphorylation, and cytoskeletal linkage of acetylcholine receptors. J Neurosci 25, 10479–10493.
Schmidt N, Basu S, Sladecek S, Gatti S, van Haren J, Treves S, Pielage J, Galjart N, Brenner HR (2012). Agrin regulates CLASP2-mediated capture of microtubules at the neuromuscular junction synaptic membrane. J Cell Biol 198, 421–437.
Schröder R, Kunz WS, Rouan F, Pfendner E, Tolksdorf K, Kappes-Horn K, Altenschmidt-Mehring M, Knoblich R, van der Ven PFM, Reimann J, *et al*. (2002). Disorganization of the desmin cytoskeleton and mitochondrial dysfunction in plectin-related epidermolysis bullosa simplex with muscular dystrophy. J Neuropathol Exp Neurol 61, 520–530.
Sealock R, Murnane AA, Paulin D, Froehner SC (1989). Immunochemical identification of desmin in Torpedo postsynaptic membranes and at the rat neuromuscular junction. Synapse 3, 315–324.
Selcen D, Juel VC, Hobson-Webb LD, Smith EC, Stickler DE, Bite AV, Ohno K, Engel AG (2011). Myasthenic syndrome caused by plectinopathy. Neurology 76, 327–336.
Strnad P, Windoffer R, Leube RE (2002). Induction of rapid and reversible cytokeratin filament network remodeling by inhibition of tyrosine phosphatases. J Cell Sci 115, 4133–4148.

Ursitti JA, Lee PC, Resneck WG, McNally MM, Bowman AL, O'Neill A, Stone MR, Bloch RJ (2004). Cloning and characterization of cytokeratins 8 and 19 in adult rat striated muscle. Interaction with the dystrophin glycoprotein complex. J Biol Chem 279, 41830–41838.
Valencia RG, Walko G, Janda L, Novacek J, Mihailovska E, Reipert S, Andrä-Marobela K, Wiche G (2013). Intermediate filament-associated cytolinker plectin 1c destabilizes microtubules in keratinocytes. Mol Biol Cell 24, 768–784.
Walko G, Wögenstein KL, Winter L, Fischer I, Feltri ML, Wiche G (2013). Stabilization of the dystroglycan complex in Cajal bands of myelinating Schwann cells through plectin-mediated anchorage to vimentin filaments. Glia 61, 1274–1287.
Wiche G, Winter L (2011). Plectin isoforms as organizers of intermediate filament cytoarchitecture. Bioarchitecture 1, 14–20.
Winter L, Abrahamsberg C, Wiche G (2008). Plectin isoform 1b mediates mitochondrion-intermediate filament network linkage and controls organelle shape. J Cell Biol 181, 903–911.
Winter L, Staszewska I, Mihailovska E, Fischer I, Goldmann WH, Schröder R, Wiche G (2014). Chemical chaperone ameliorates pathological protein aggregation in plectin-deficient muscle. J Clin Invest 124, 1144–1157.
Winter L, Wiche G (2013). The many faces of plectin and plectinopathies: pathology and mechanisms. Acta Neuropathol 125, 77–93.
Wu H, Xiong WC, Mei L (2010). To build a synapse: signaling pathways in neuromuscular junction assembly. Development 137, 1017–1033.
Yang J, Dominguez B, de Winter F, Gould TW, Eriksson JE, Lee KF (2011). Nestin negatively regulates postsynaptic differentiation of the neuromuscular synapse. Nat Neurosci 14, 324–330.
Zhang B, Luo S, Dong XP, Zhang X, Liu C, Luo Z, Xiong WC, Mei L (2007). Beta-catenin regulates acetylcholine receptor clustering in muscle cells through interaction with rapsyn. J Neurosci 27, 3968–3973.
Zörner B, Filli L, Starkey ML, Gonzenbach R, Kasper H, Röthlisberger M, Bolliger M, Schwab ME (2010). Profiling locomotor recovery: comprehensive quantification of impairments after CNS damage in rodents. Nat Methods 7, 701–708.